UNITED REPUBLIC OF TANZANIA
Ministry of Energy and Minerals (MEM)
Dodoma

BUNDESREPUBLIK DEUTSCHLAND
Bundesanstalt für Geowissenschaften und Rohstoffe (BGR)
Hannover

Promoting the Development of Geothermal Energy Tanzania

Structural analysis of Mt. Meru and the surrounding area based on Remote Sensing data

Dr. Kai Hahne

Hannover, August 2017

Structural analysis of Mt. Meru and the surrounding area based on Remote Sensing data

Author	Dr. Kai Hahne (BGR)

Commissioned by	Federal Ministry for Economic Cooperation and Development (BMZ: Bundesministerium für wirtschaftliche Zusammenarbeit und Entwicklung)
Project Number	BMZ PN 2013.2250.2
BGR Number	05-2364
Implementing Agencies	MEM (Ministry of Energy and Minerals); TGDC (Tanzania Geothermal Development Company Federal Institute for Geosciences and Natural Resources (BGR: Bundesanstalt für Geowissenschaften und Rohstoffe, Hannover)
Pages	48
Place and date of issuance	Hannover, August 2017

Table of Contents

Abbreviations

ASTER GDEM	Advanced Spaceborne Thermal Emission and Reflection Radiometer Global Digital Elevation Map. (Digital Elevation Model; combination of ASTER-Satellite data and SRTM data)
BGR	Bundesanstalt für Geowissenschaften und Rohstoffe (Federal Institute for Geosciences and Natural Resources)
DEM	Digital Elevation Model
DTM	Digital Terrain Model
GIS	Geographic Information System
GPS	Global Positioning System
m asl	Metres above sea level
MEM	Ministry of Energy and Minerals
OLI	Operational Land Imager (Sensor on board of Landsat 8 Satellite)
Pmax	Maximum principal stress
Pmin	Minimum principal stress
RGB	Red Green Blue (colour band combination)
SRTM	Shuttle Radar Topography Mission
TGDC	Tanzanian Geothermal Development Company
TM	Thematic Mapper (Sensor on board of Landsat 5 Satellite)
TerraSAR-X (TSX)	German high resolution RADAR-Satellite
WP	Way Point (Measured by GPS)

List of figures

Summary

A structural analysis based on multispectral satellite data as well as on high- and medium resolution DEMs improve the geological and tectonic knowledge of a working area within the framework of a geothermal exploration programme.

The working area at Mt. Meru is situated in the Northern Tanzanian Divergence Zone. Three rifts of different orientations, creating complicated regional and local stress fields, dominate this area.

The mapped lineaments represent faults, strongly connected to the youngest movements of the ongoing rifting of the Neogene rifts. Some lineaments form X-shaped conjugated faults, displaying the regional stress field and the present opening direction of the Natron-Manyara-Rift, which likely displays the recent dominant rift-direction.

Faults of WNW orientations dominate the Mt. Meru area. Along these orientations, young hydrothermal alterations occur in the crater of the central ash cone.

East of Mt. Meru, a concentration of intersections of all existing fault orientations is found, making this area highly permeable for any fluids and is possibly a location for further examinations.

There are structural hints –to my knowledge not mentioned so far in literature- which strongly suggest the existence of a NW-SE orientated graben structure between Mt. Meru and Mt. Kilimanjaro (inferred “Meru Kilimanjaro Graben”). This “Meru Kilimanjaro Graben” would represent the “Mt. Kilimanjaro-deflected” prolongation of the Pangani Graben.

Lake Momella represents very likely a former, now (debris avalanche-) eroded crater.

1 Scope of the Work

Within the bilateral project “Geothermal Energy Development Tanzania” between BGR and the “Tanzanian Geothermal Development Company” (TGDC), the approach lies upon the estimation of the potential for hydrothermal energy at Mount Meru.

A structural analysis of Mt. Meru and its surrounding area contributes to this aim by improving the tectonic/geological understanding of the working area. Faults of different ages, which can act as pathways for hydrothermal features can be detected as linear features (lineaments) at the earth´s surface.

As vast parts of the working area are vegetated, steep and difficult to access, remote sensing in combination with focused ground truth is an excellent method to meet the requirements for structural mapping. The analysis is based on high- and medium resolution digital elevation models (DEM) and multispectral data.

A first field-scoping mission in combination with a planning workshop in Arusha has been conducted together with partners of TGDC from 17/10/2016 to 26/10/2016. Findings of the field-scoping mission were presented at the workshop.

2 Working Area

The core working area for the geothermal exploration programme comprises Mt. Meru and its closest vicinity (Fig. 2.1, yellow frame, Fig. 2.2). For structural analyses, it is necessary to consider also the surrounding area with its variety of tectonic features (Fig. 2.1).

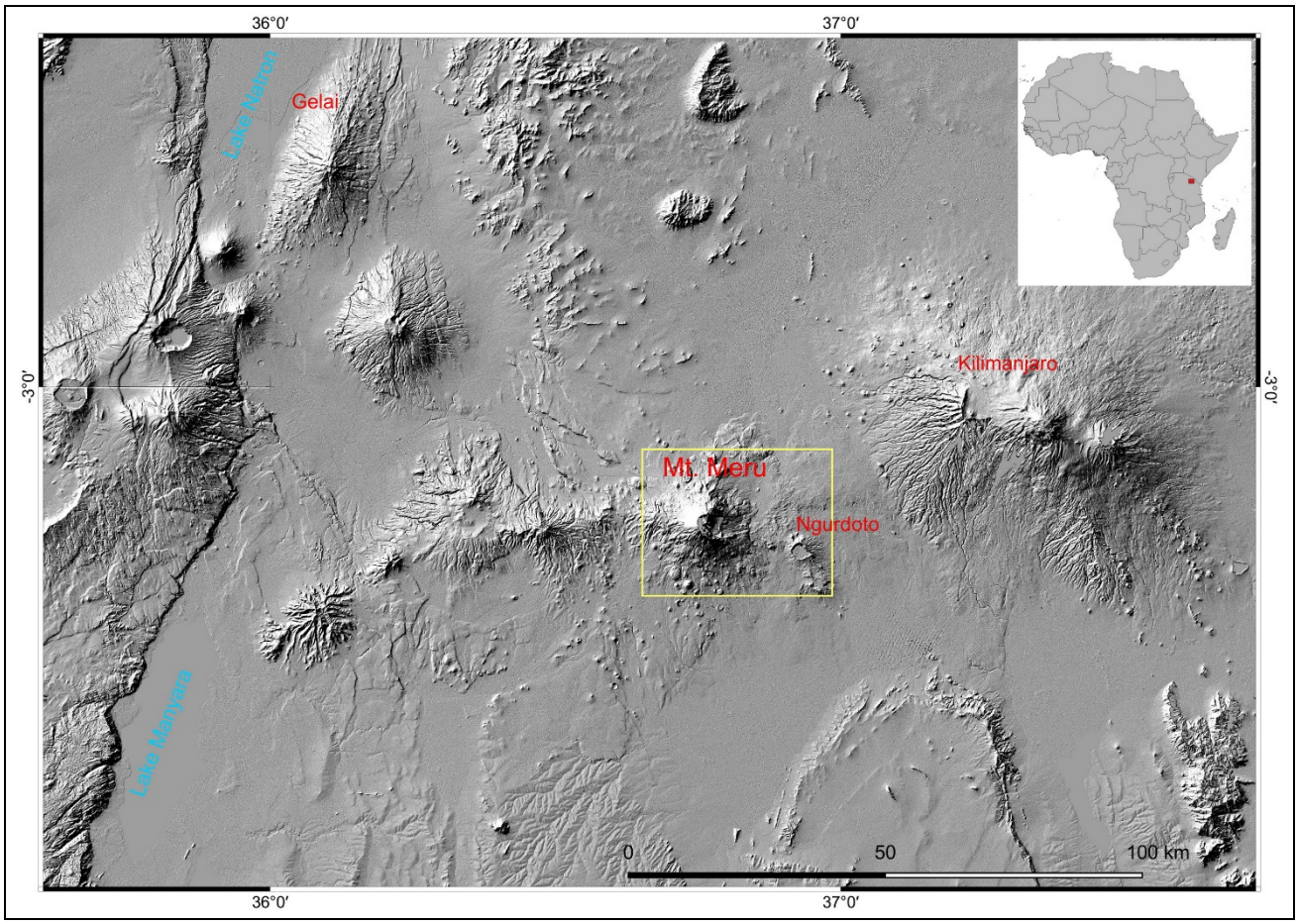

Figure 2.1: The major working area and the location of the core working area at Mount Meru (yellow frame) in Tanzania. 30 m SRTM elevation model shaded relief.

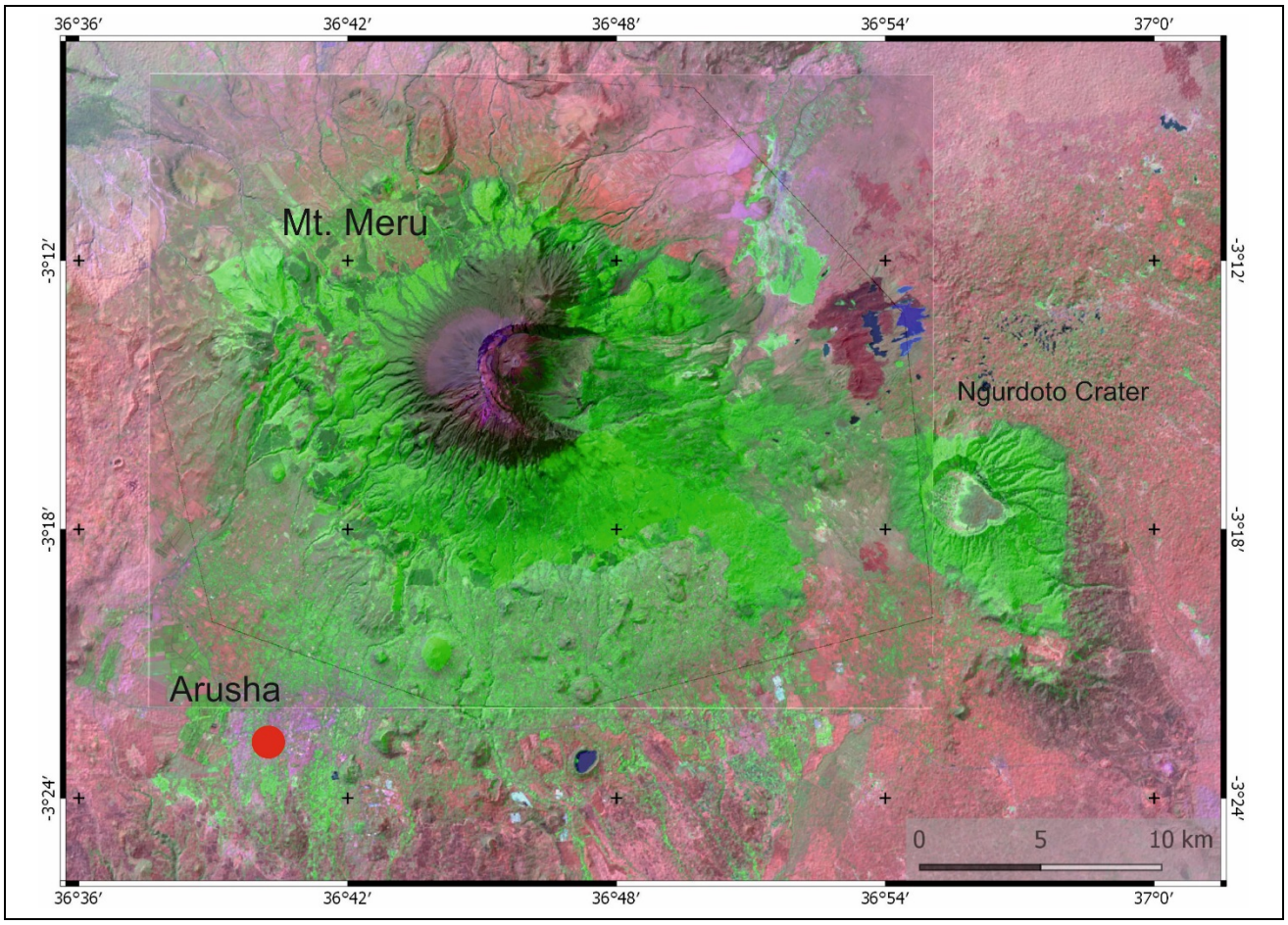

Figure 2.2: The working area with Mt. Meru. Landsat TM bands 7,4,1 (RGB). Projected onto high resolution 12m TerraSAR-X WorldDEM (Mt. Meru area only) and 30m SRTM DEM shaded relief.

3 Data

The following data were used within Quantum GIS (version 2.18.2) for further analysis and lineament vectorization:

- Enhanced and geocoded satellite images:
    - Landsat TM (30m ground resolution) acquired February, 02, 2000,
    - Landsat OLI (30m ground resolution) acquired January, 08, 2016,
    - Landsat OLI (30m ground resolution) acquired March, 10, 2016,
    - Landsat OLI (30m ground resolution) acquired August, 03, 2016,
    - Aster GDEM 30m digital elevation model,
    - SRTM 30m digital elevation model,
    - TerraSAR-X WorldDEM 12m digital elevation model.
- Geocoded raster data:
    - Geological map Arusha Quarter Degree Sheet 55 (WILKINSON, P. ET AL. 1983).
- Information from overview-field work (4 days only):
    - Shape and visibility of lineaments,
    - Additional geological and tectonic information,
    - Field photos,
    - Waypoints (WP) of findings and locations of photo documentations from GPS measurements.

The spatial reference system used for this study is UTM 37 S, WGS 84.

The following layers have been created:

- Lineaments
- Normal Faults
- Normal Faults Assumed
- Mt. Meru Slope Angles (0°-90°) based on TerraSAR-X WorldDEM
- Shaded relief Maps from all available DEMs

- Waypoints with corresponding data tables concerning information from field work (lithology, photos etc.).

The data including additional field photos with locations not mentioned in this report are attached on DVD to this report as a Quantum GIS-project. In figures, that show field photos, the location refers to a GPS waypoint (WP). All waypoints are listed in a table and a corresponding map in the appendix to allow traceability of the field survey.

4 Geology

The core working area around Mount Meru is situated in the Northern Tanzanian Divergence and is built up of Precambrian rocks of the Tanzania Craton (Archaean) and the north-south trending Mozambique orogenic fold belt (Archean/Proterozoic, BEECKMANS, B., 2014, DAWSON (2008), Fig. 4.1). The Tanzania Craton has an elevation of over 1100 m. This reflects the existence of a subcratonic plume whose effects can be seen in the volcanics of both branches of the rift system (BEECKMANS, B., 2014).

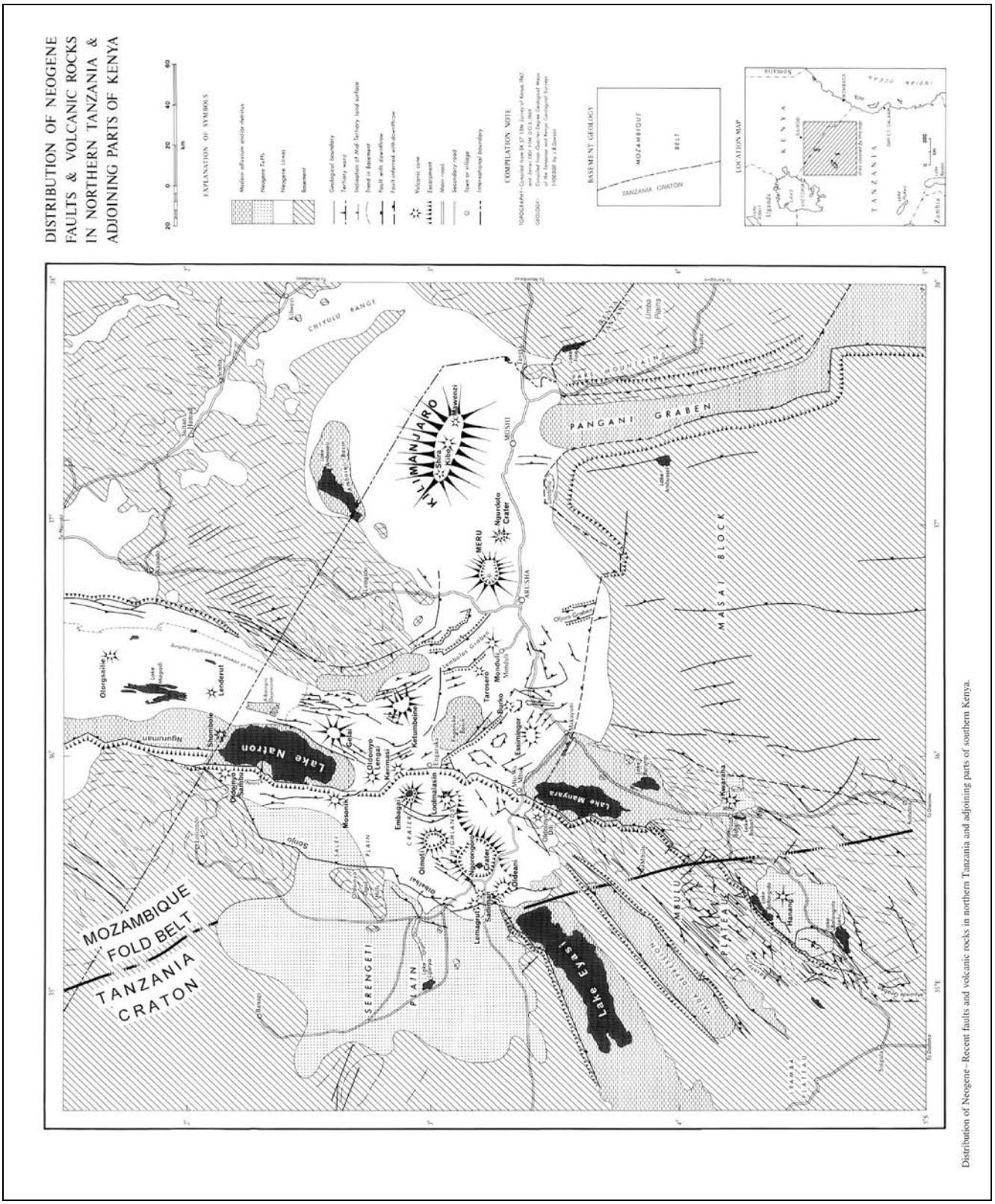

Figure 4.1: The Northern Tanzanian Divergence, DAWSON (2008).

4.1 Precambrian

The rocks of the Tanzania Craton represent three formations:

1. Kavirondian,
2. Nyanzan and
3. Dodoman.

They consist of Archaean metasediments, which were intruded by granites and migmatised during three short tectono-metamorphic events (BEECKMANS, B., 2014).

The Mozambique Fold Belt was formed during the Usagaran metamorphic event by subduction at the southeastern end of the Tanzania Craton (QUENNELL ET. AL. 1956 in BEECKMANS, B., 2014). The Mozambique Fold Belt represents a polycyclic orogenic complex, whose last event ended 650 Ma B.P.

The rocks of the Mozambique Fold Belt comprise two major series:

1. The higher Crystalline Limestone Series with quartzites, dolomitic marbles, graphitic marble, graphites, mica schists, kyanite gneisses and metabasites (QUENNELL ET. AL. 1956 in BEECKMANS, B., 2014) and
2. The lower Masai Series with quartzo-feldspatic gneisses, charnockites and hornblende-biotite gneisses (Fig. 4.2).

Figure 4.2: Precambrian gneiss transported from the deeper subsurface and exposed by the eruption of (Cenozoic) Mungu Crater, SW of Mt. Meru (WP 23).

4.2 Cenozoic

Mount Meru – a 4565m high stratovolcano – and its surrounding area is built up of multi-phase volcanic products as flood basalts (Fig. 4.5) - which represent the oldest - lavas, pyroclastics and lahars (Figures 4.3, 4.4), which were reinterpreted as debris avalanches by DELCAMP ET. AL. (2016). All these volcanites overlie the Precambrian basement.

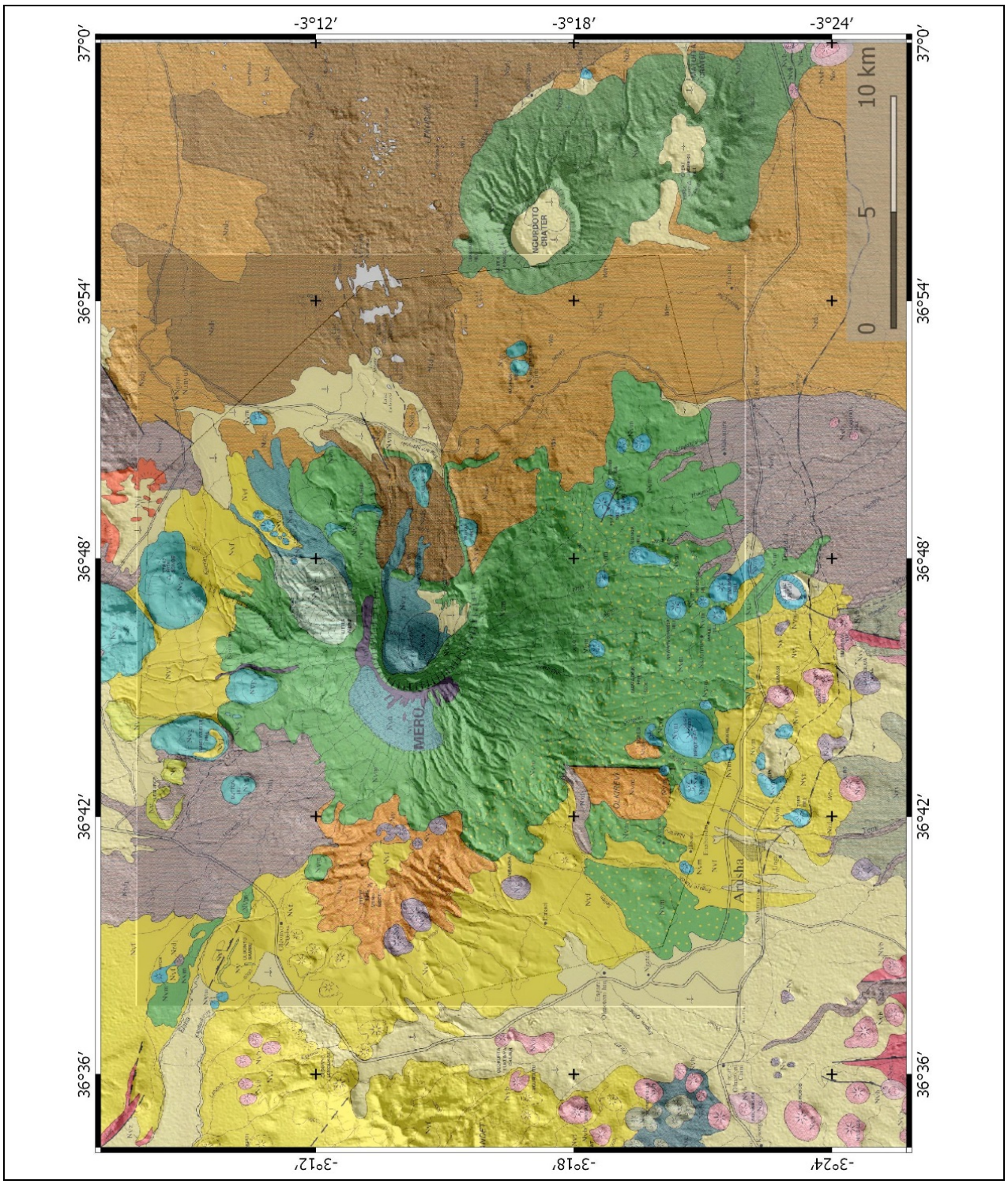

Figure 4.3: The Geology of Mt. Meru area after WILKINSON, P. ET AL. (1983) projected onto TSX WorldDEM and SRTM DEM, shaded relief. Legend see next figure.

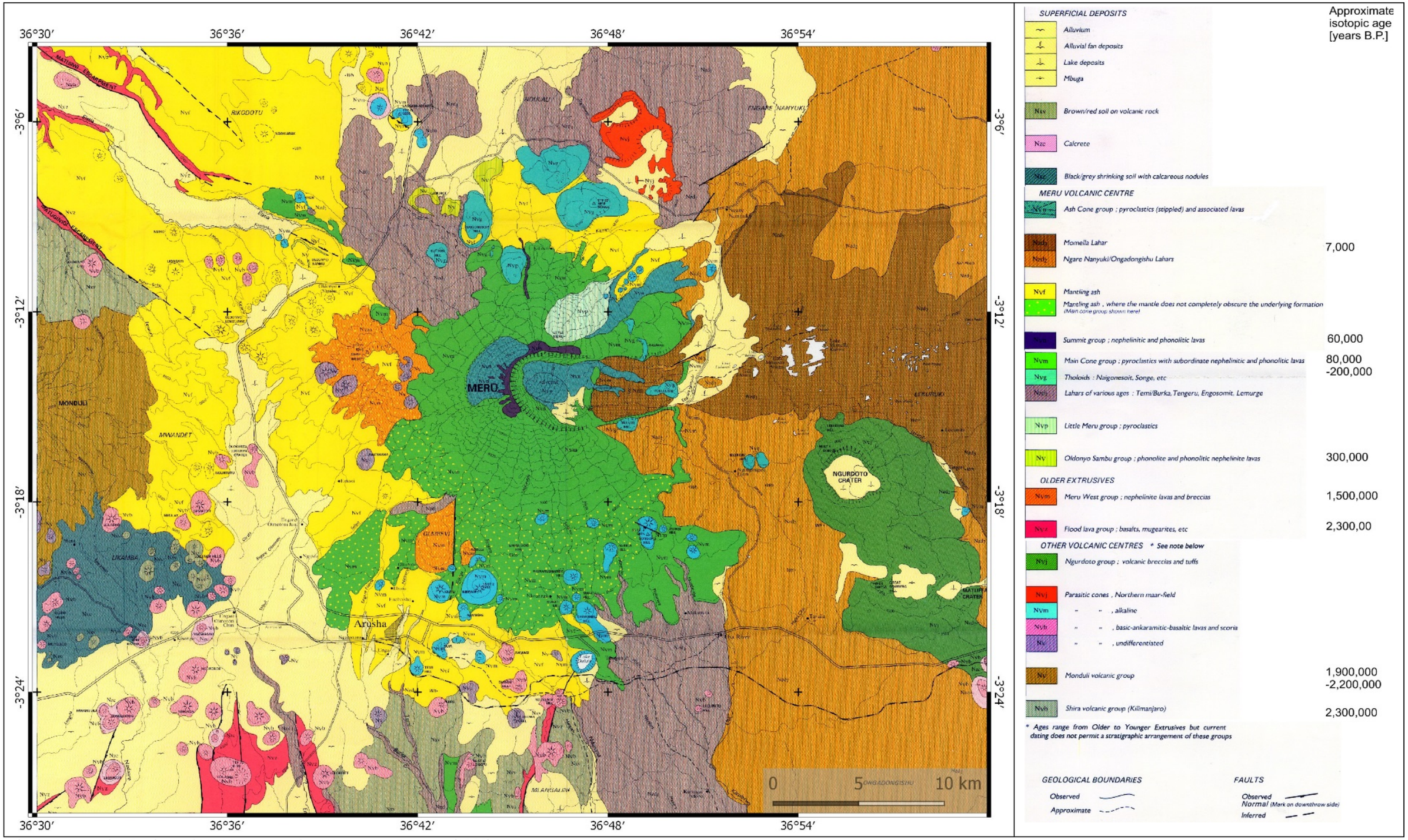

Figure 4.4: The Geology of Mt. Meru area after WILKINSON, P. ET AL. (1983).

Figure 4.5: Flood basalt outcrop exposed in a vertical profile of Mungu Crater, SW of Mt. Meru (WP 26).

A striking feature of Mt. Meru is the missing eastern flank (Fig. 4.6). This typical horseshoe-shaped scar formed after a sector collapse of Mt. Meru approximately 8600 years B.P. (SIEBERT, L., 1984) respectively 7000 years B.P. (after WILKINSON, P. ET AL., 1983), depositing huge debris avalanches (DELCAMP ET. AL., 2016) (described as “lahars” by WILKINSON, P. ET AL., 1983). These debris avalanches reach out to the lower slopes of Mt. Kilimanjaro to the east and cover approximately 1500 km^2 (WILKINSON, P. ET AL., 1983). ROBERTS (2002) calculated the volume of the debris avalanches to 28 km^3 by modelling the pre-collapse surface of Mt. Meru.

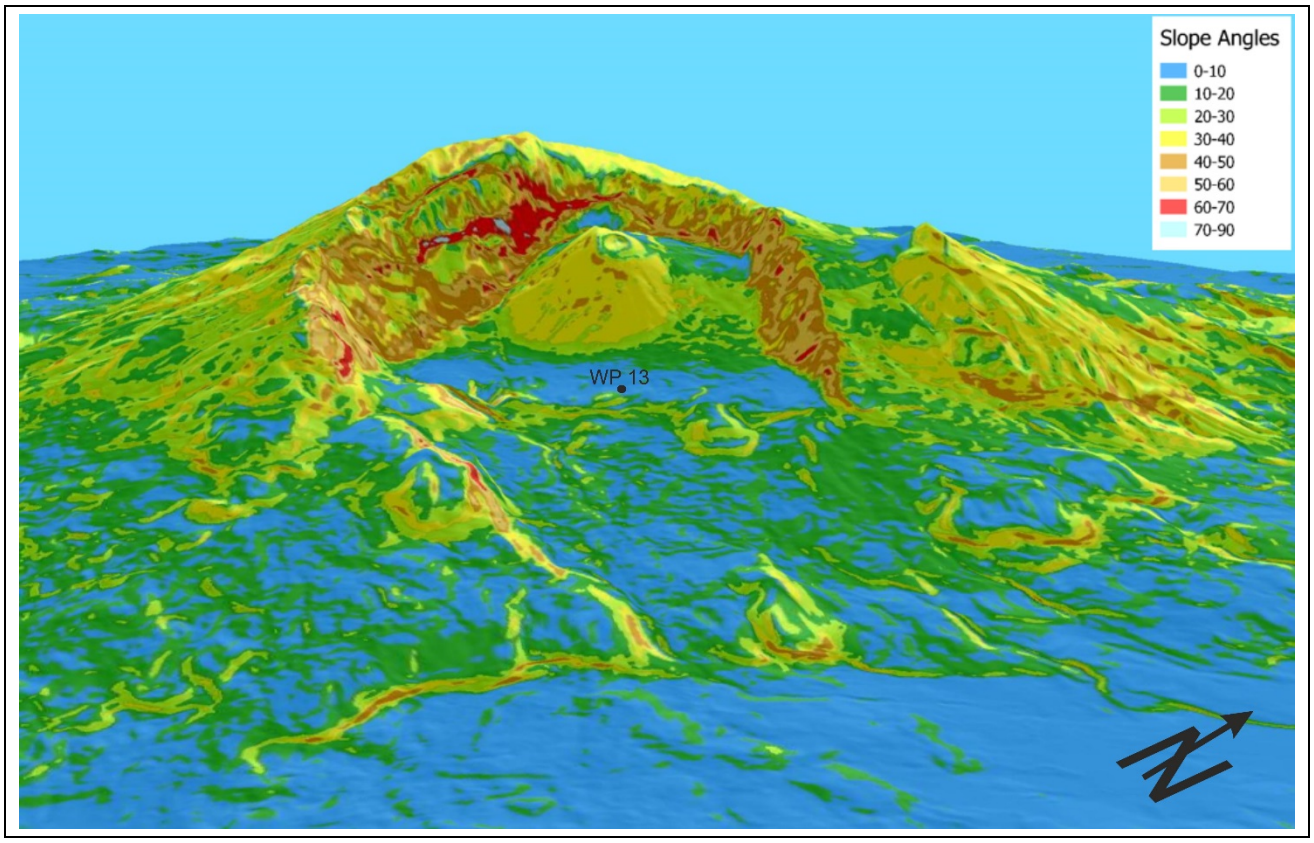

Figure 4.6: The collapsed eastern flank of Mt. Meru. Slope angle map derived from TSX WorldDEM projected over TSX DTM shaded relief. Perspective view into the crater with the central ash cone. 1.5 X vertical exaggeration. WP 13 indicates the position of the field photo (see figure 4.7).

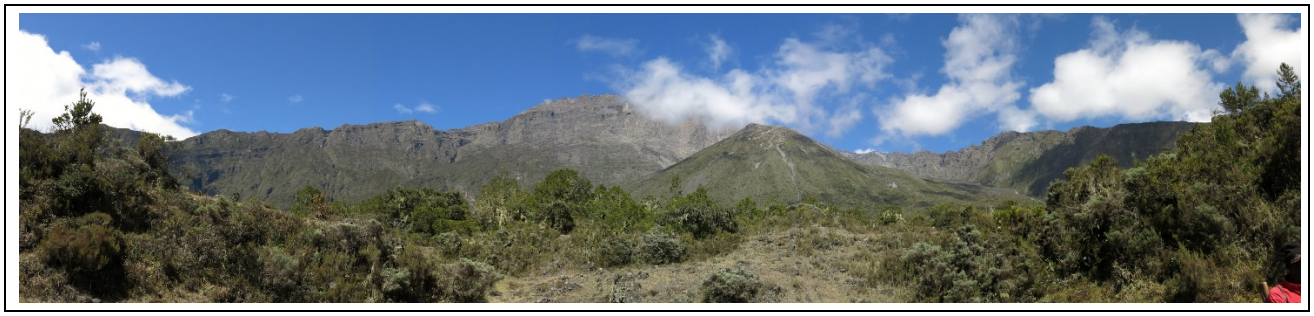

Figure 4.7: Mt. Meru crater with the central ash cone, view to the west, from WP 13 (see figure 4.6).

Mt. Meru is an active volcano, which last erupted black ash from the central ash cone (Figures 4.6, 4.7 and 4.8) in 1910, furthermore, significant fumarolic activity was recorded 1954 in the central ash cone (Fig. 4.9) and might have ceased before 1974 (WILKINSON, P. ET AL., 1983). Warm, mineralised springs (23°C) are present especially in the eastern crater area (Fig. 4.10).

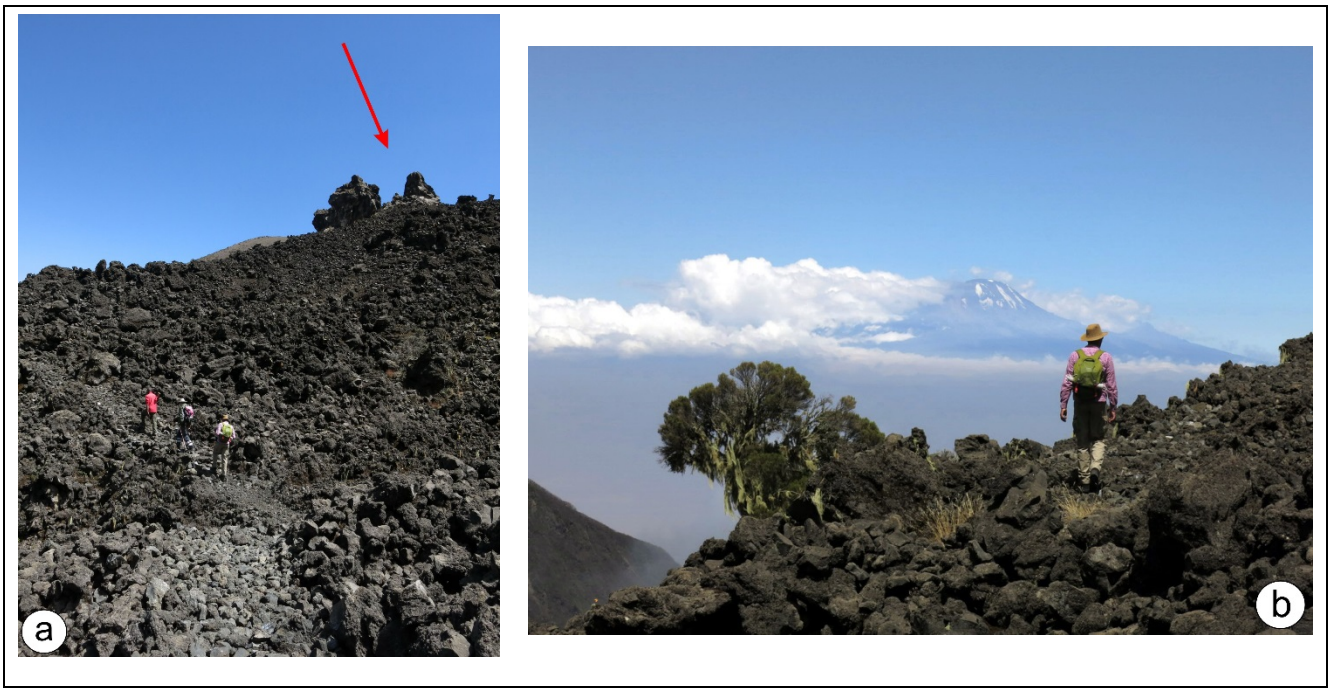

Figure 4.8: a: Youngest lavas of the Ash Cone Group with lava dome (red arrow), view to the south, WP9. b: Youngest lavas of the Ash Cone Group. View to the east with Mt. Kilimanjaro in the background.

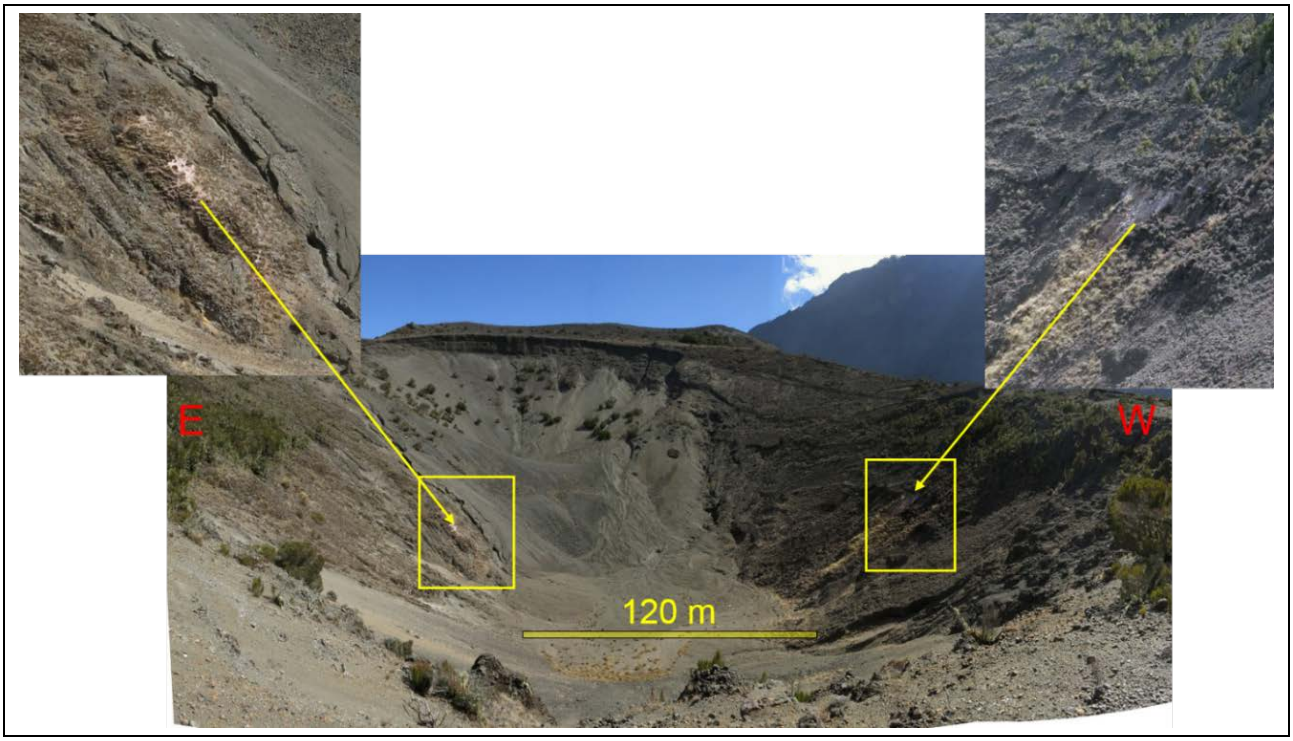

Figure 4.9: Hydrothermal alterations at the inner west- and east flanks of the inner ash cone´s crater. View to the south, WP11.

Figure 4.10: Warm spring (23° C) in the eastern crater area, WP18.

5 Tectonic setting

Three distinct rifts with different orientations (FOSTER ET AL., 1997) dominate the working area in the Northern Tanzanian Divergence Zone:

1. The Natron-Manyara-Balangida Rift (N-S-trending),
2. the Eyasi-Wembere Rift (NE-trending) and
3. the Pangani Rift (NW-trending).

The rifts are named after the lakes, which have developed on the rift bottoms. They transect the lithospheric boundary between the Archean (Tanzania Craton) and the Proterozoic (Mozambique orogenic fold belt), (Figure 4.1). An example of tectonics of Archean rocks is shown in figures 5.1 and 5.2, where multiphase folding is observed (orange lines). The NW trending Pangani Graben is built up by rocks of the Proterozoic Mozambique orogenic fold belt.

The orientations of the major rifts and the orientations of aligned volcano-chains (Fig. 5.2), are variable and display the changing tectonomagmatic conditions and are a result of the interplay between:

- The regional stress field,
- the local magma-induced stress field and
- stress rotations by mechanical interaction of rift segments (MUIRHEAD ET. AL., 2015).

The intrusion of aligned volcanic-chains (Figure 5.2) widely follows Precambrian basement structures and (reactivated) faults.

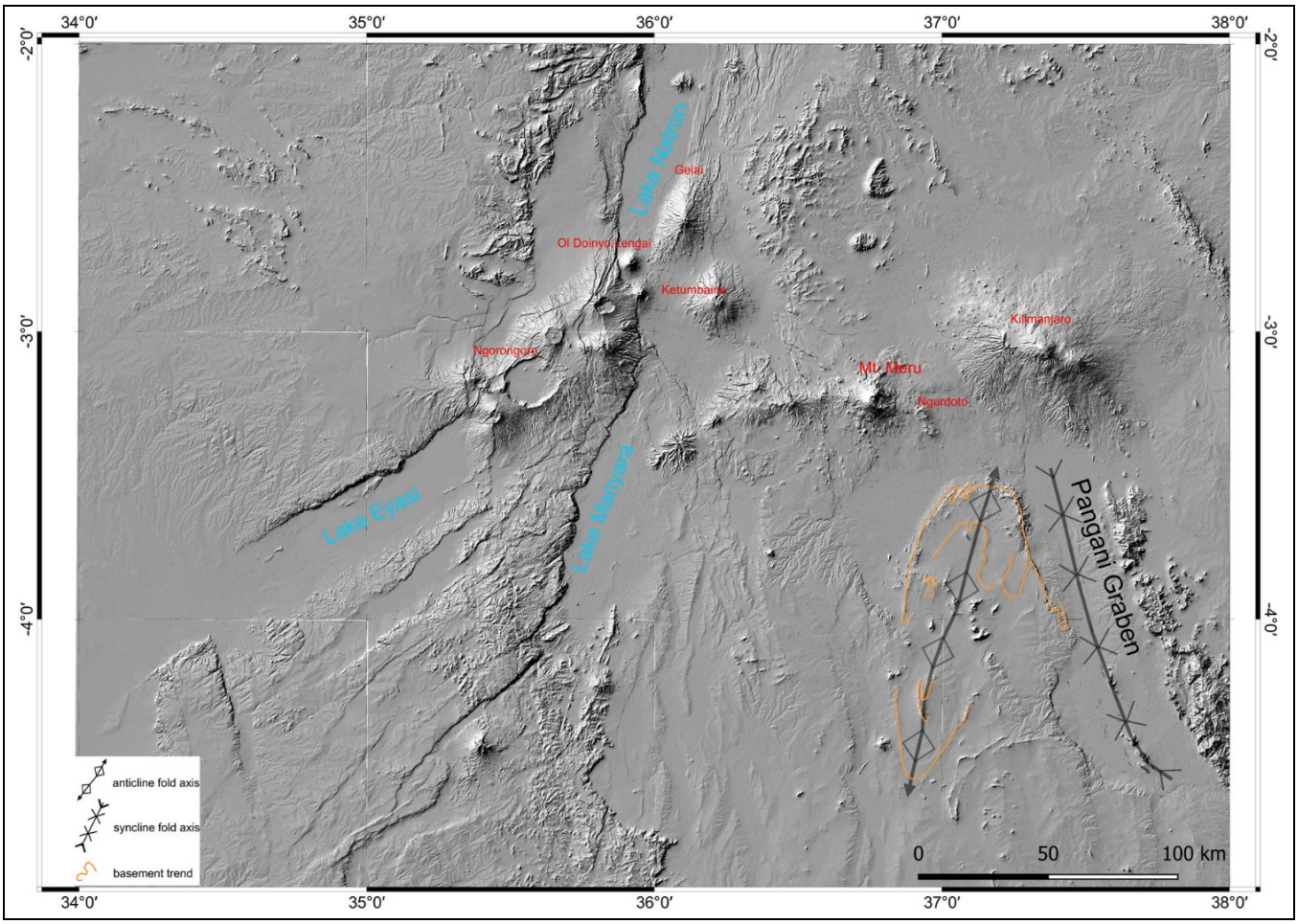

Figure 5.1: Northern Tanzanian Divergence Zone with Natron-Manyara-, Eyasi- and Pangani rifts (named after the lakes often developed on the rift bottoms) with different orientations. One example for Archean basement structures, which shows multiphase folding is highlighted by orange lines. The NW trending Pangani Graben is built up by rocks of the Proterozoic Mozambique orogenic fold belt. Shaded relief SRTM DEM mosaic.

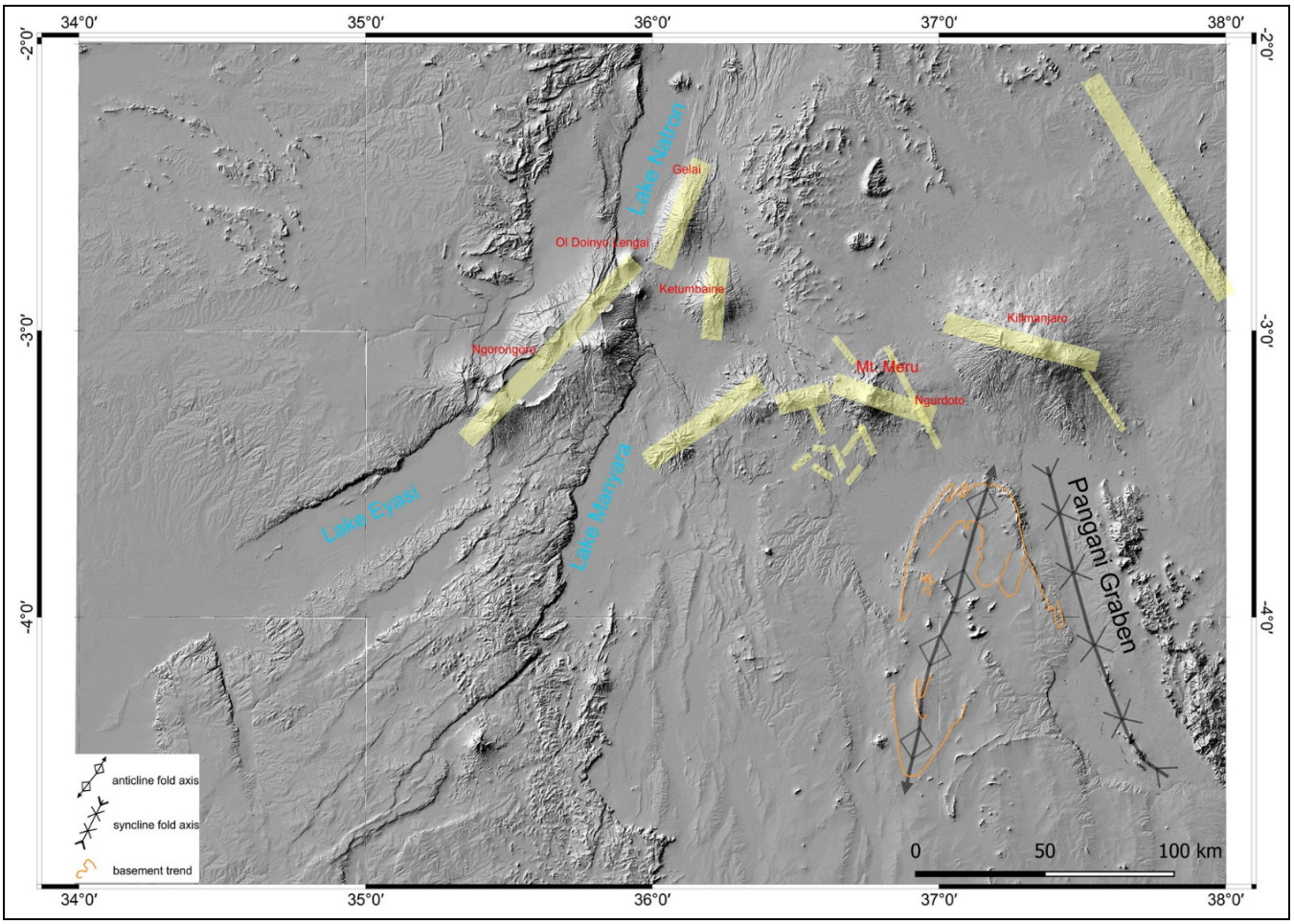

Figure 5.2: The variable orientations of aligned volcano-chains (yellow stripes showing examples) display the changing tectonomagmatic conditions. The intrusion widely follows Precambrian basement structures and (reactivated) faults. One example for Archean basement structures, which shows multiphase folding is highlighted by orange lines. The NW trending Pangani Graben is built up by rocks of the Proterozoic Mozambique orogenic fold belt. Shaded relief SRTM DEM mosaic.

5.1 Lineaments

The majority of the mapped lineaments represent faults (Fig. 5.3). Wherever possible, “normal faults” were distinguished from other “lineaments”. They are strongly connected to the ongoing rifting of the Neogene rifts. Normal faults impressively offset older shield volcanoes as Gelai and Ketumbaine (Fig. 5.4). This faulting follows a NE direction at Gelai and turns to a NW direction slightly farther south at Ketumbaine, displaying the change of the structural trends of the Precambrian basement (see also Figure 4.1).

At the inner northern crater flank of Mt. Meru, some lineaments can be attributed to a dyke intrusion of the pyroclastics of the Main Cone Group (Fig. 5.5).

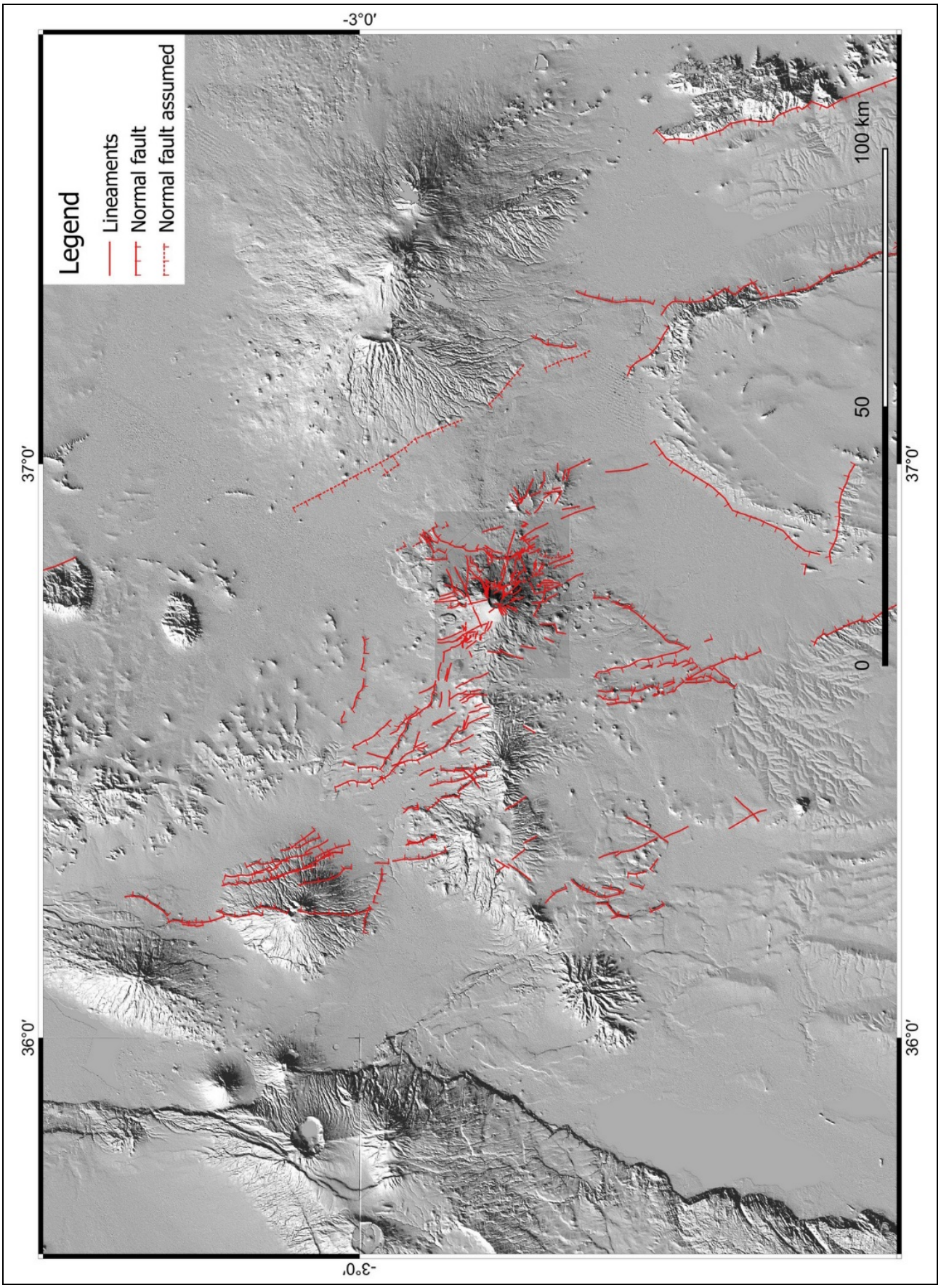

Figure 5.3: Examples for lineaments and normal faults (assumed normal faults, to be explained later below) in the major area of Mount Meru. Shaded relief SRTM DEM mosaic.

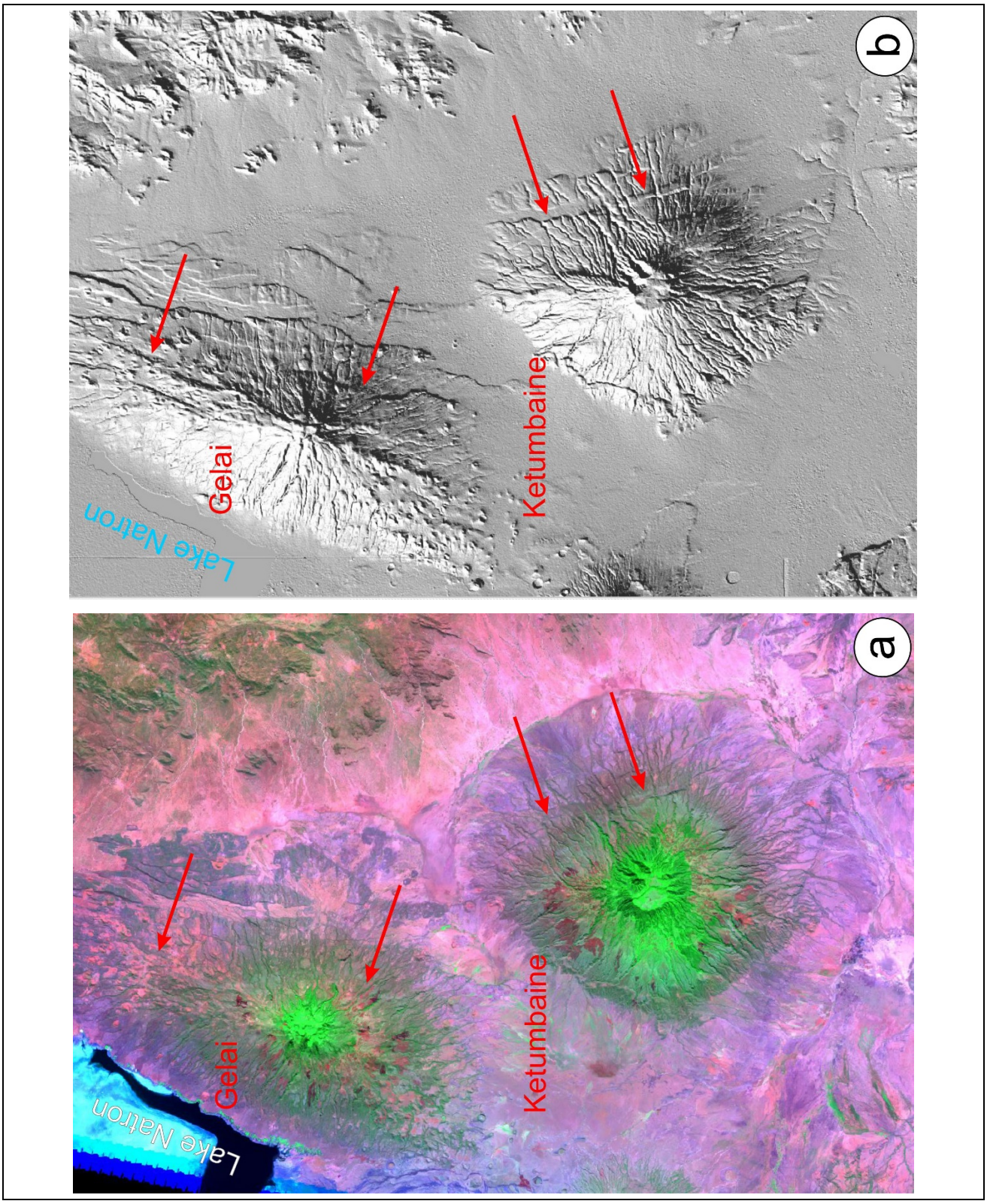

Figure 5.4: The shield volcanoes Gelai and Ketumbaine are offset by normal faulting (red arrows showing examples), which turns from a NE- at Gelai to a NW direction at Ketumbaine (red arrows). This can be attributed to a change of the structural trend of the Precambrian basement (see Fig. 4.1). a: Landsat TM bands 7,4,1 (RGB) supply spectral information about the surface´s character: “false colours” e.g. cyan: salt crust of Lake Natron, black: clear water, pink: bare rock/soil. green: vegetation. b: shaded relief 30m SRTM DEM enhances structures like faults (red arrows, examples).

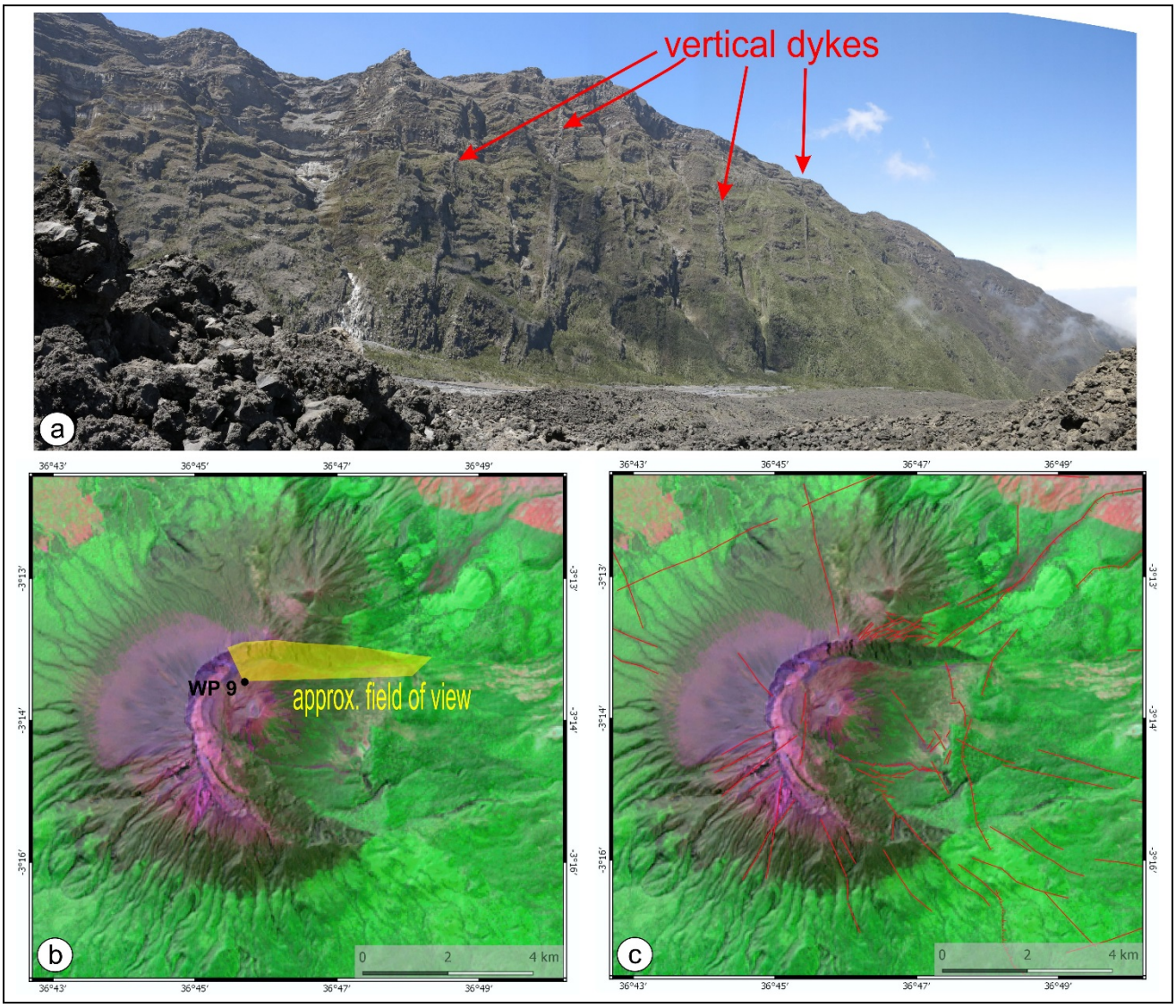

Figure 5.5: At the inner northern flank of Mt. Meru, some mapped lineaments can be attributed to a dyke intrusion of the pyroclastics of the Main Cone Group. a: Field Photo, view to NE (WP9). b: The approximate field of view of the field photo (a). c: Mapped lineaments at Mt. Meru. Landsat OLI, bands 7,5,3 (RGB).

Some lineaments form X-shaped conjugated faults, displaying the regional stress field and the present opening direction of the Natron-Manyara-Rift. This direction most likely displays the recent dominant rifting (Fig. 5.6).

Lineament mapping was focused to the core Mt. Meru area and to a certain extent also to the surrounding area outside Mt. Meru to examine and exemplify fault- and lineament directions in a larger framework. All directions of the dominant rifts are reflected also inside the relatively small working area (Figures 5.7, to 5.11). The orientations of the *assumed* normal faults were not considered in the rose diagrams. The rose diagrams are not weighted by lineament lengths.

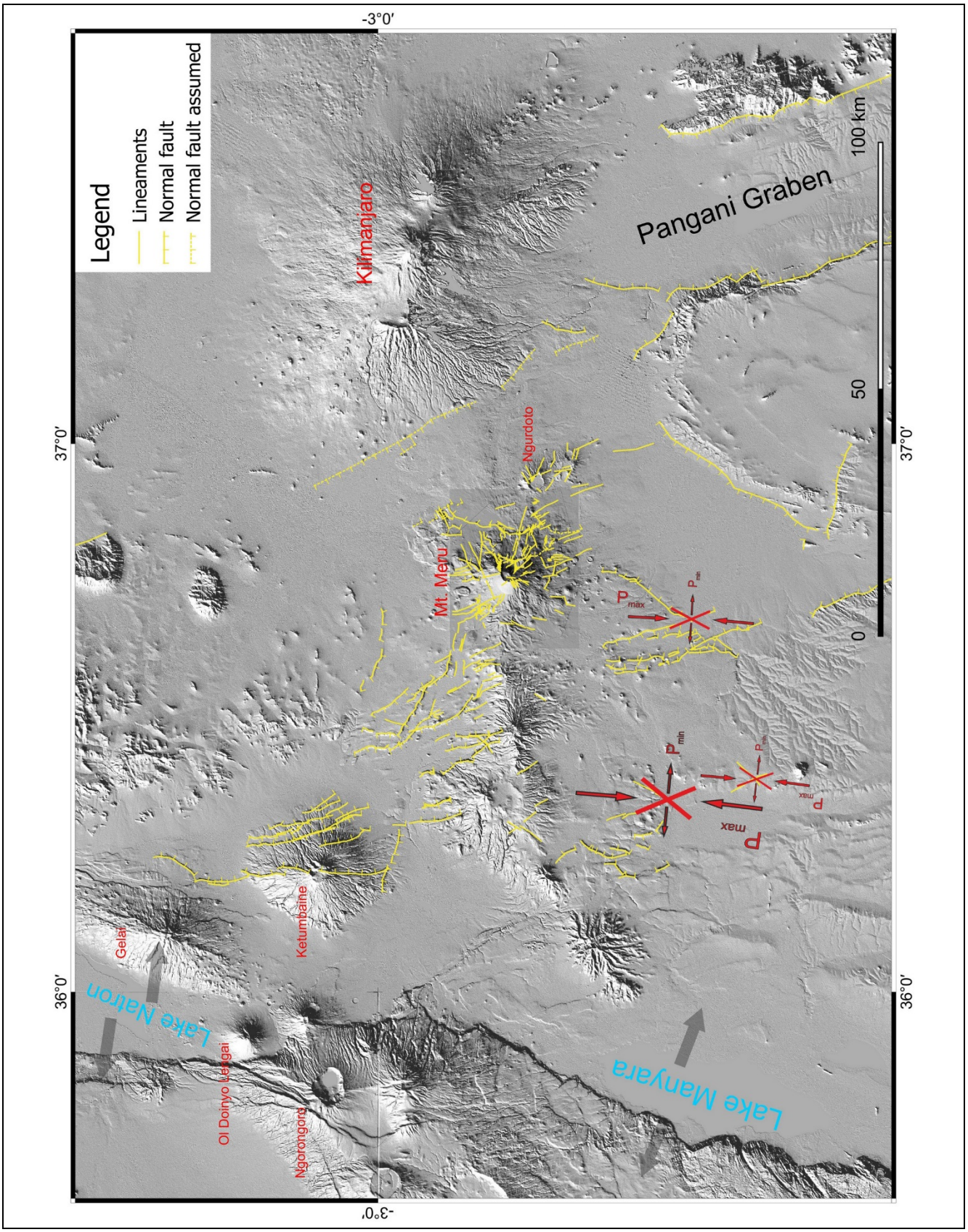

Figure 5.6: The directions of maximum principal stress can be derived from satellite imagery, regarding the X-shaped stress indicators (red lines). The acute angle between conjugated faults (red lines, three examples of more existing) is bisected by the maximum principal stress direction (P_{max}). The direction of effective minimal principal stress direction (P_{min}) corresponds in this example approximately to the opening direction of the Natron-Manyara-Rift (grey arrows).

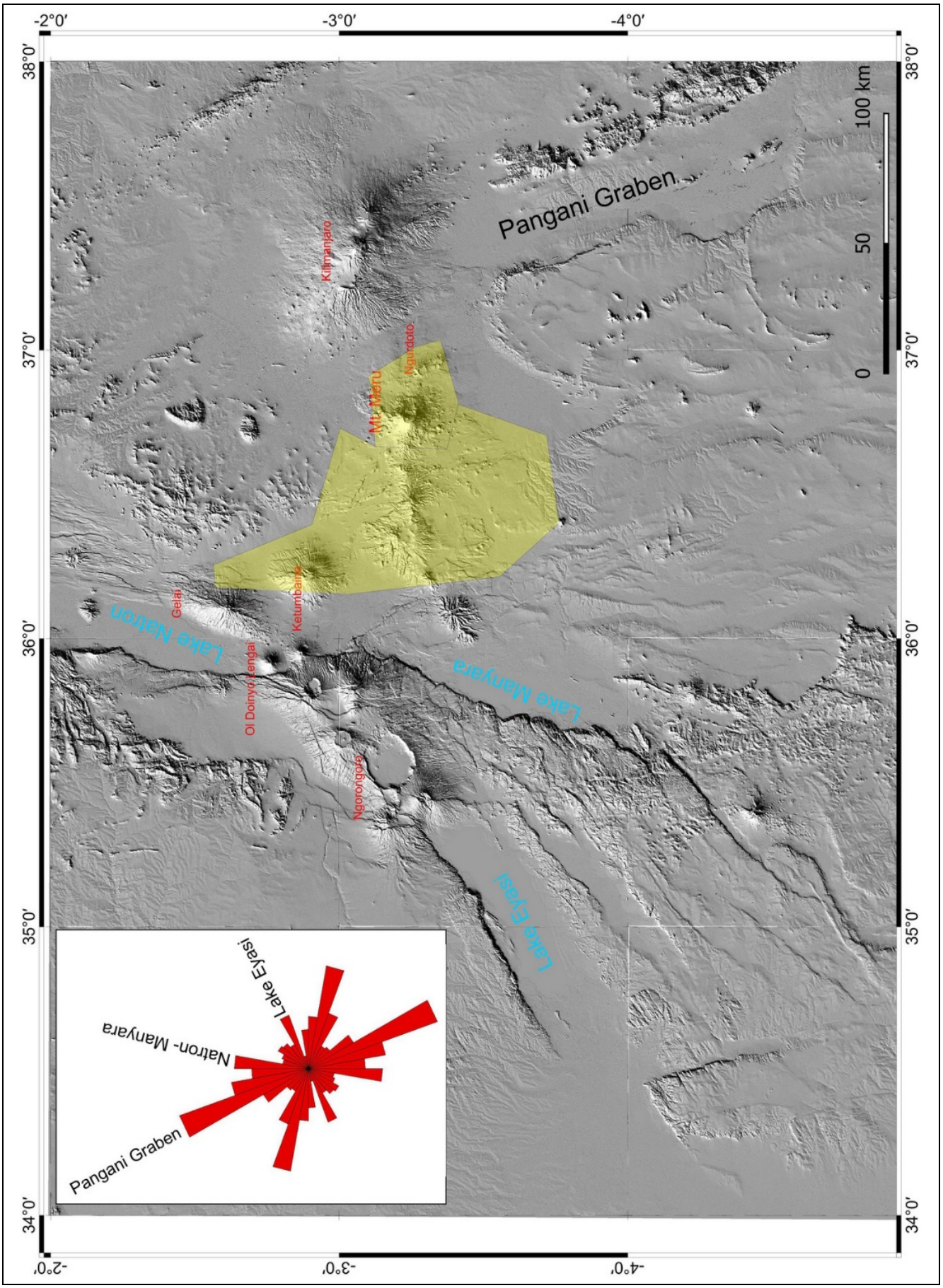

Figure 5.7: The orientations of the dominant regional rifts (Pangani Graben, Natron-Manyara and Lake Eyasi) are reflected in the extended working area (yellow polygon).

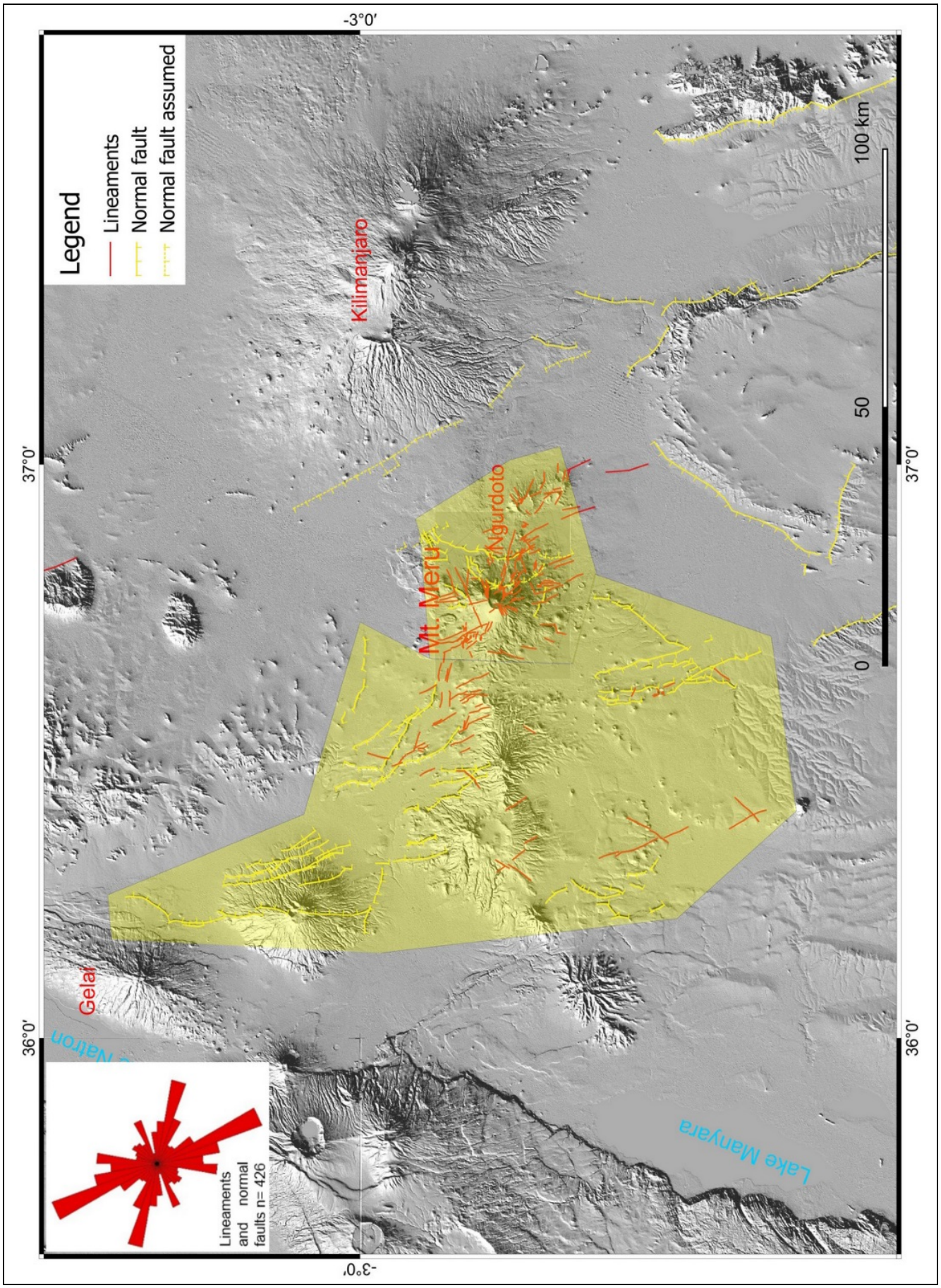

Figure 5.8: Lineaments and normal faults with rose diagram of the extended working area (yellow polygon).

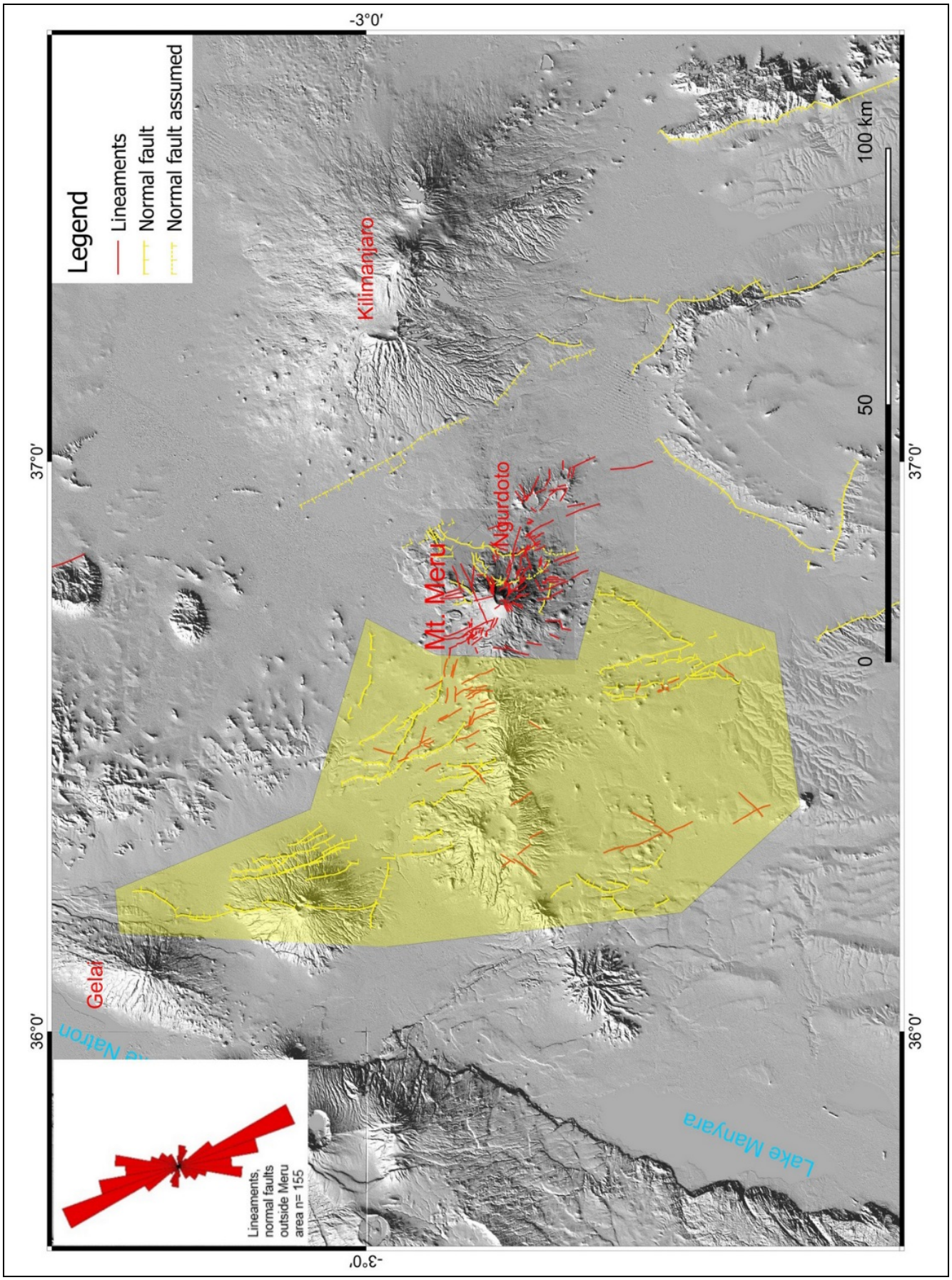

Figure 5.9: Lineaments and normal faults with rose diagram of the working area outside the “core area” of Mt. Meru (yellow polygon). The NW-SE-orientation following the Pangani Graben is the dominant fault orientation.

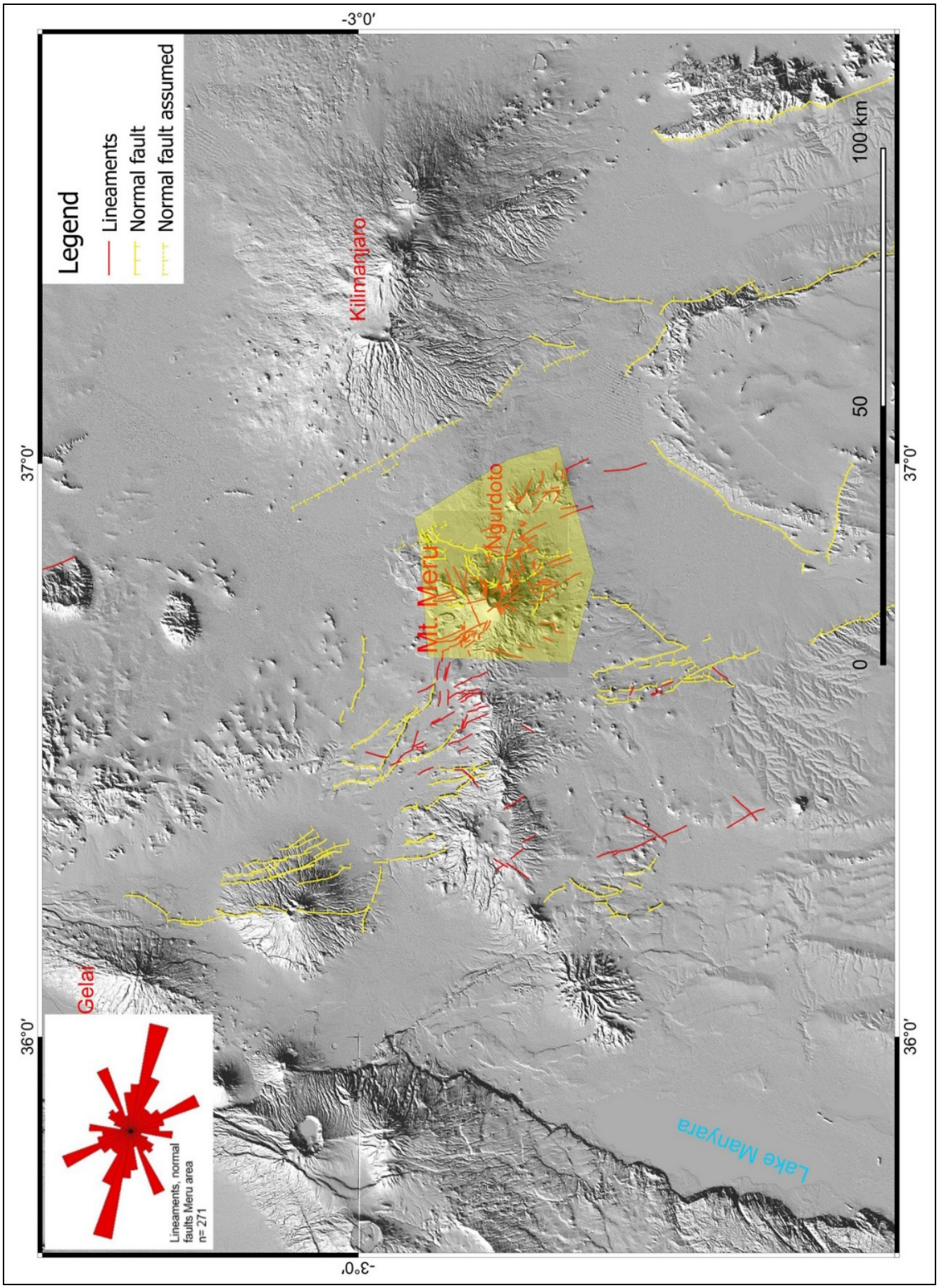

Figure 5.10: Lineaments and normal faults with rose diagram of the “core area” of Mt. Meru (yellow polygon). WNW-ESE orientations dominate this area.

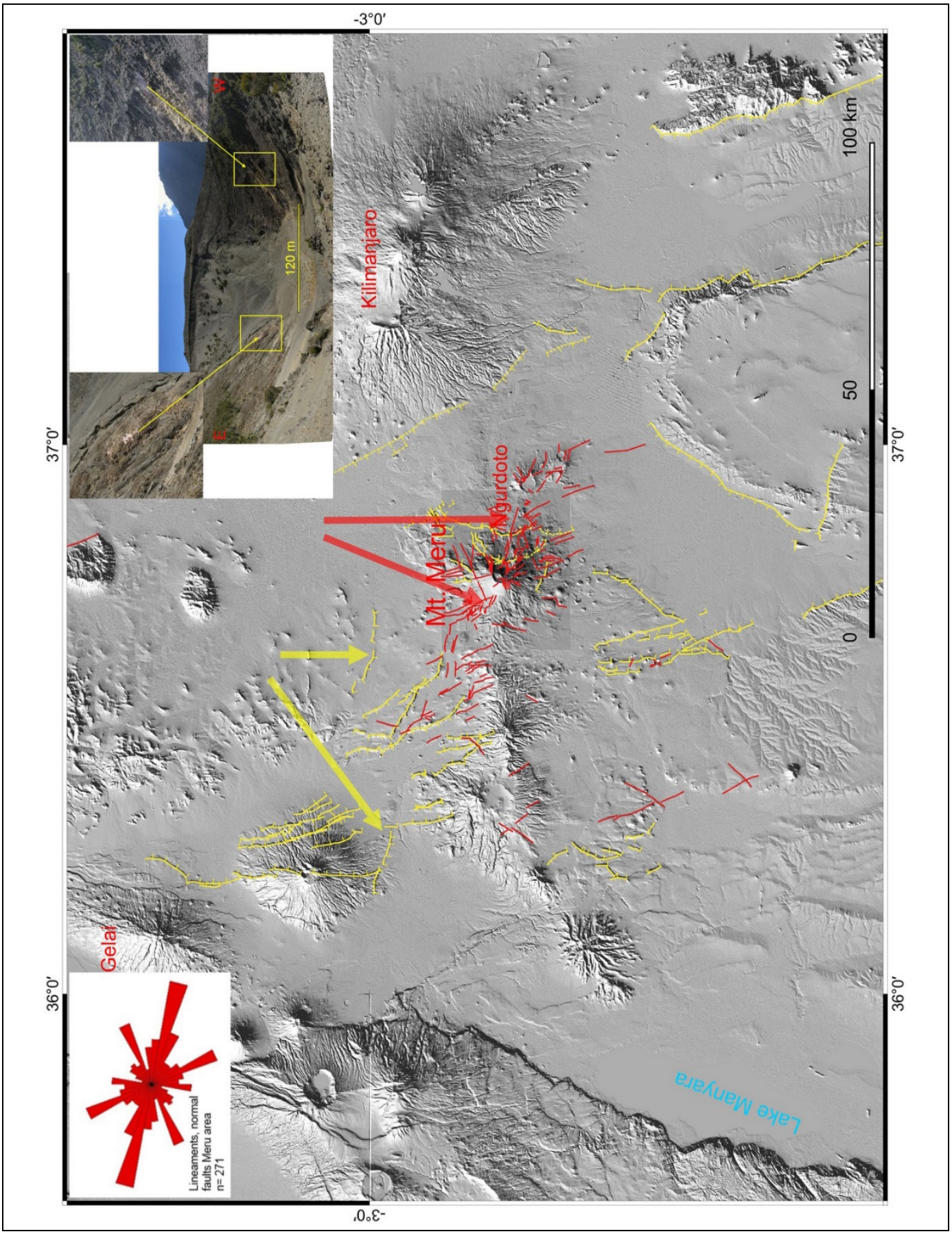

Figure 5.11: Lineaments and normal faults with rose diagram of the “core area” of Mt. Meru (yellow polygon). WNW-ESE orientations dominate this area. The inset shows hydrothermal alterations of the inner ash cone corresponding to this direction.

The direct Mt. Meru area is affected by all orientations of re-activated faults, which can also be found in the surrounding area. WNW-ESE orientations are dominant. This orientation shows hydrothermal alteration in the inner ash cone (Fig. 5.11, see also larger field photo in Fig. 4.9).

East of Mt. Meru two major bended normal faults occur (Figures 5.12 and 5.13). The western one might have triggered the Ngare Nanyuki/Ongadongishu Lahars (reinterpreted as debris avalanches). It forms a steep step at the eastern crater rim and is partially covered by a small part of a later debris flow, which is attributed to the Momella Lahar (Fig. 5.12, dark brown colour, reinterpreted as debris avalanche).

The eastern normal fault might have triggered the Momella Lahar (reinterpreted as debris avalanche), as it widely offsets the older debris avalanche and seems to affect the Momella Lahar (reinterpreted as debris avalanches) only to a minor extent (Figures 5.12, 5.13).

The discontinuous bending of the fault traces show rift orientations of the active Natron-Manyara-, Eyasi- and Pangani-Rifts.

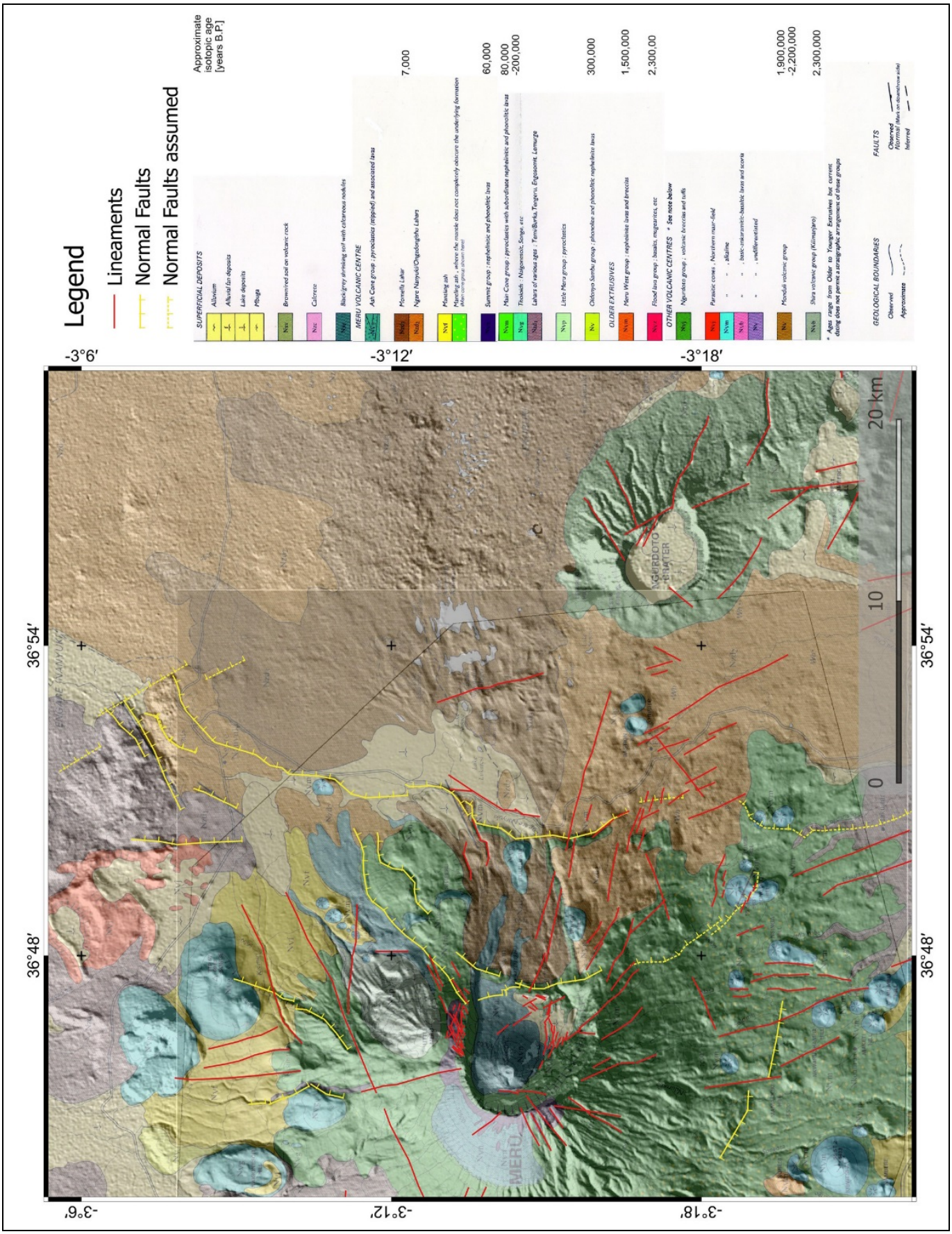

Figure 5.12: Two major bended normal faults east of Mt. Meru, which possibly have triggered the debris avalanches. Geological map (WILKINSON, P. ET AL., 1983) over shaded relief DEMs.

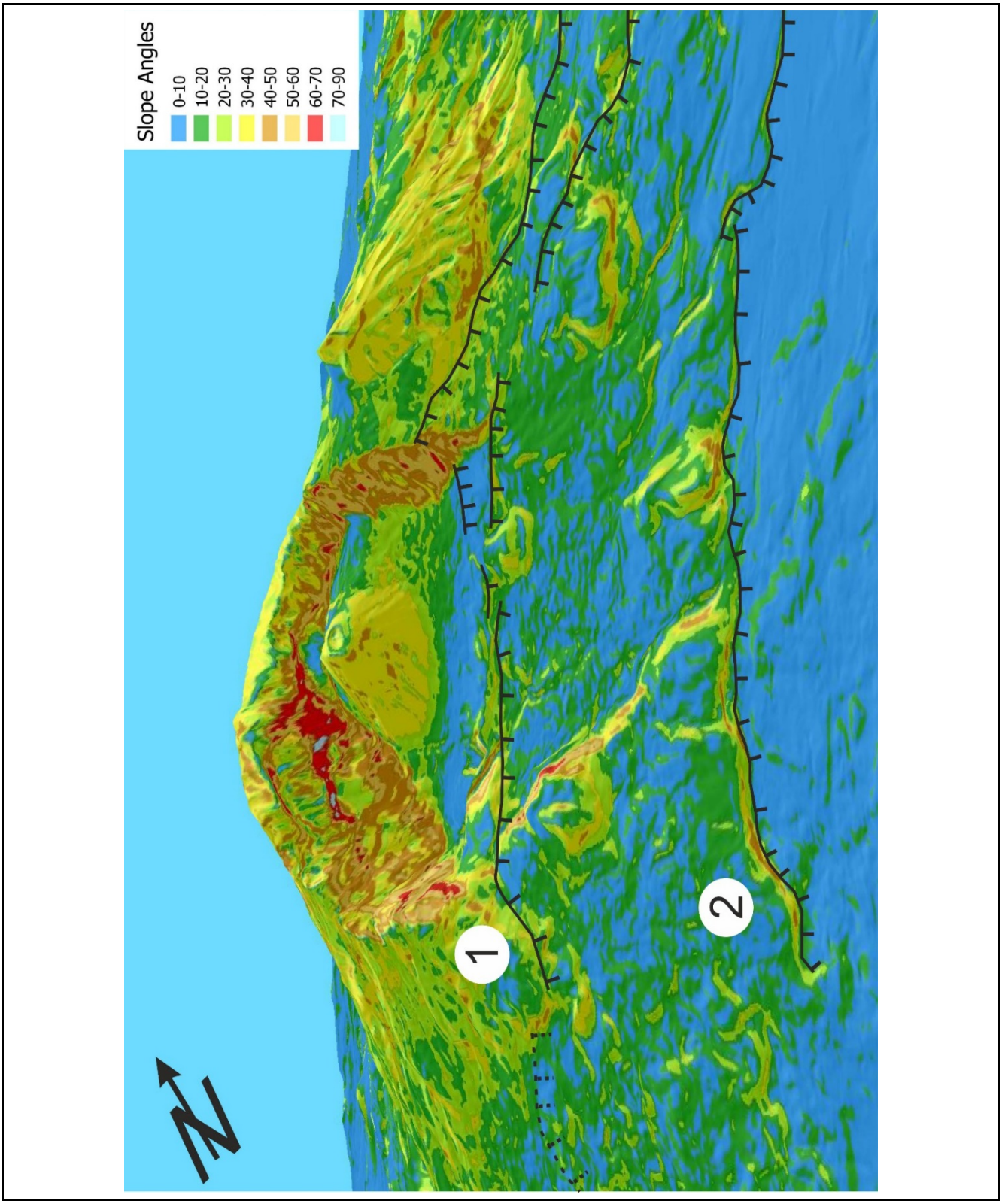

Figure 5.13: Two major bended normal faults east of Mt. Meru, which possibly have triggered the 1) Ngare Nanyuki/Ongadongishu Lahar (reinterpreted as debris avalanche) and led to the collapse of the eastern flank and 2) the Momella Lahar (reinterpreted as debris avalanches). Slope angle map derived from TSX WorldDEM projected over TSX DTM shaded relief. Perspective view into the crater with central ash cone to the west. 1.5 X vertical exaggeration.

5.2 Graben Structures

Many Graben structures in the surrounding area of Mt. Meru have NW-SE orientations like the dominant Pangani Graben. Some have flanks with chains of aligned volcanoes like the Oljoro Graben (Fig. 5.14). Aligned volcanoes reflect faults of the deeper basement also in other places (Fig. 5.16).

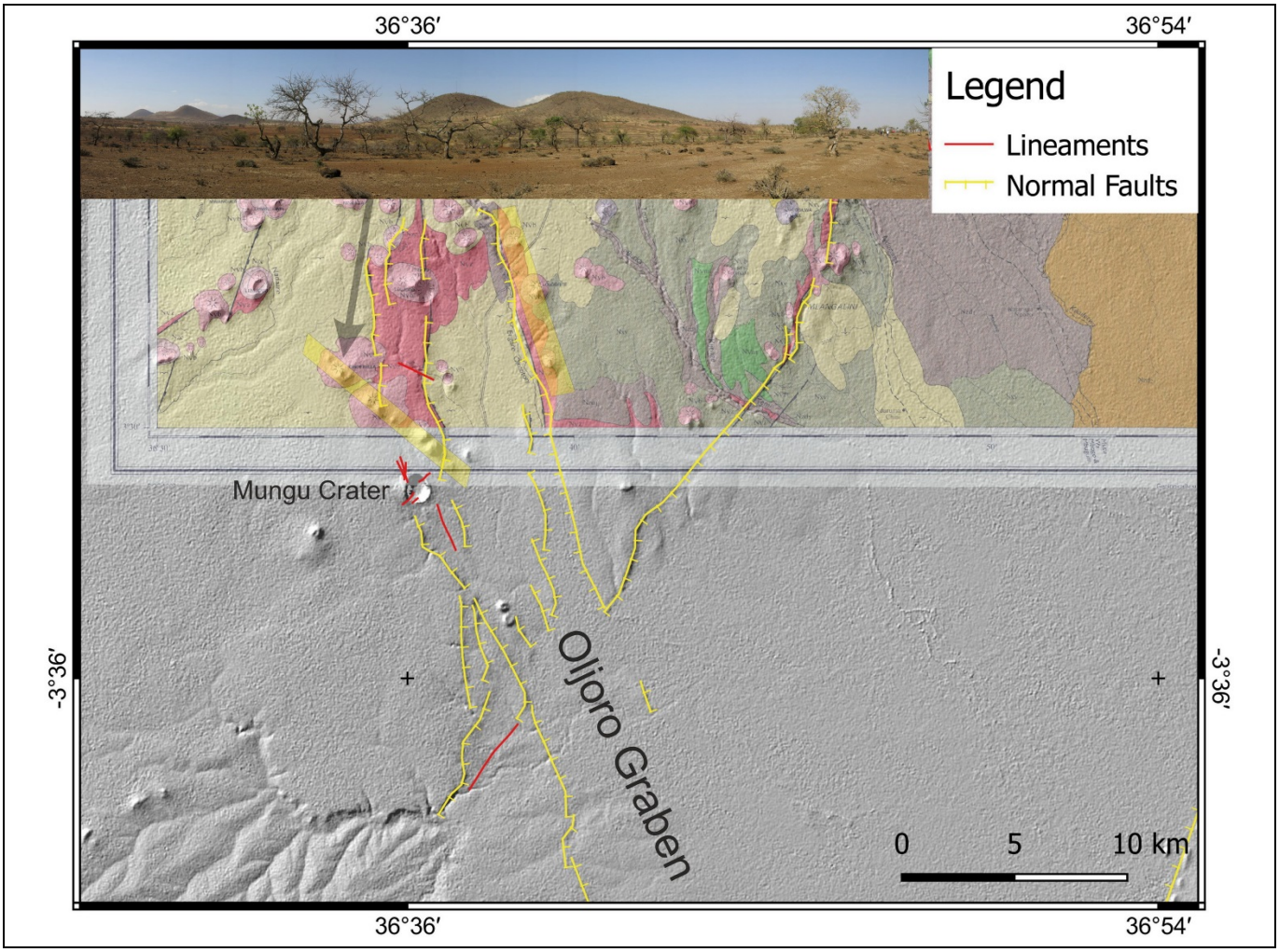

Figure 5.14: The NW-oriented Oljoro Graben with volcano-chains running parallel and NW-angular towards the flanks (transparent yellow stripes). The inset shows the angular volcanic chain as seen from Mungu Crater. Subset of the geological map (WILKINSON, P. ET AL., 1983) over shaded relief DEM.

There are structural hints, which strongly suggest the existence of a NW-SE orientated graben structure between Mt. Meru and Kilimanjaro (inferred “Meru Kilimanjaro Graben”). The shaded relief DEM clearly shows a (debris avalanche-filled) depression with linear borders. The western flank is covered with the major “volcanic-chain” of Ngurdoto crater and others (Fig. 5.15), the eastern flank at the foot of Mt. Kilimanjaro shows only minor aligned cones, which cut the inferred fault in similar NW-angles as at the western flank of the Oljoro Graben (Fig. 5.14, transparent yellow stripes). At the southern end of the assumed normal fault is an occurrence of hot springs (Fig. 5.15a, red dot).

The postulated “Meru Kilimanjaro Graben” would represent the “Mt. Kilimanjaro-deflected” prolongation of the Pangani Graben. The structure possibly runs even farther to NE, what is suggested by an eastward tilted block north of the town of Namanga/Kenya (Fig. 5.16). LE GALL ET. AL. (2008) attribute this block to be part of the Aswa shear zone running NW from the eastern shoulder of the Pangani Graben through Mt. Kilimanjaro.

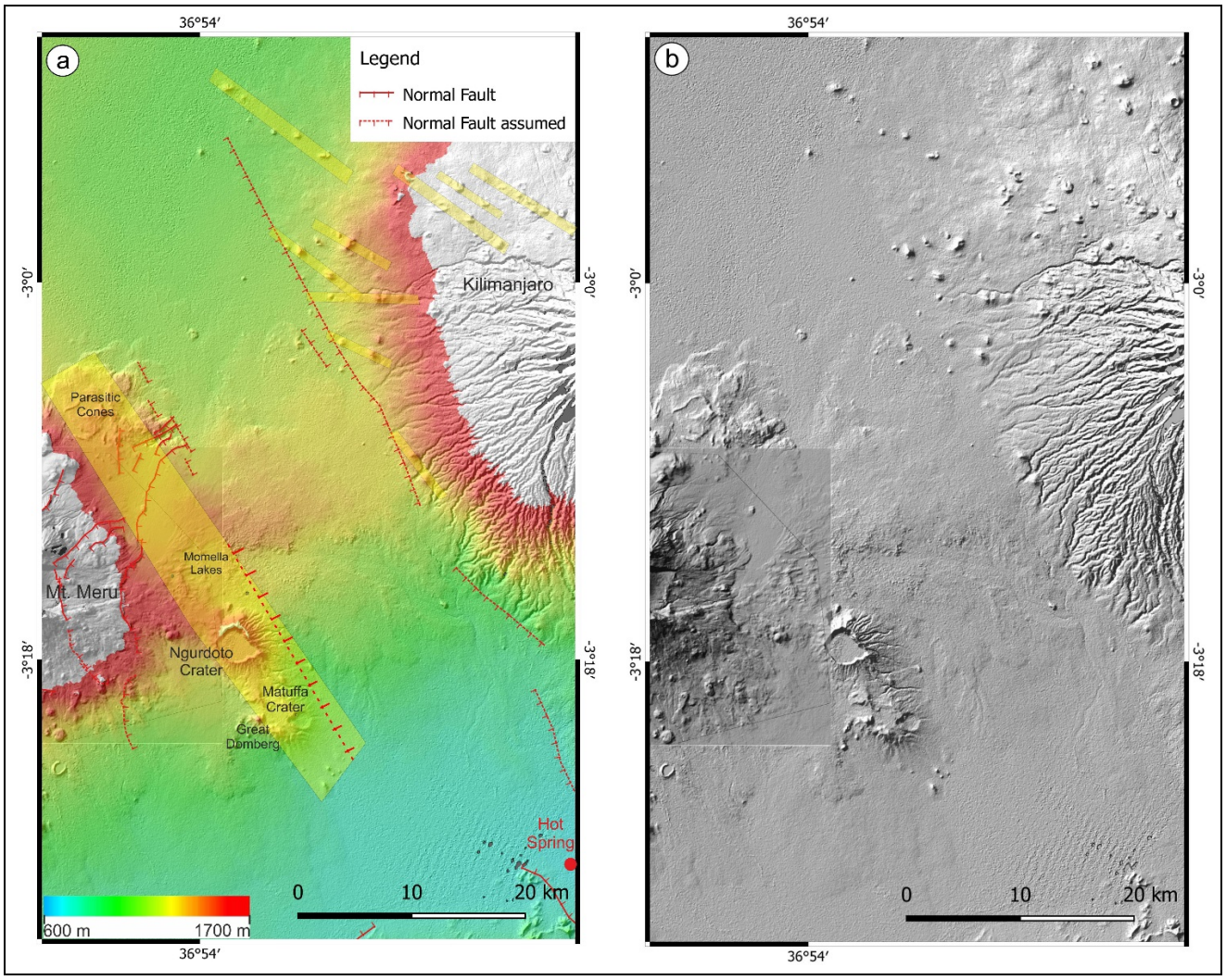

Figure 5.15: a: The NW-oriented graben structure between Mt. Meru and Kilimanjaro with normal faults, assumed normal faults and volcanic-chains (transparent yellow stripes along the flanks. The topographic heights inside the structure represent the debris avalanches emerging from Mt. Meru. Colour coded DEM over shaded relief DEMs. b: The un-interpreted shaded relief DEMs reveal the linear graben structure between Mt. Meru and Mt. Kilimanjaro even better.

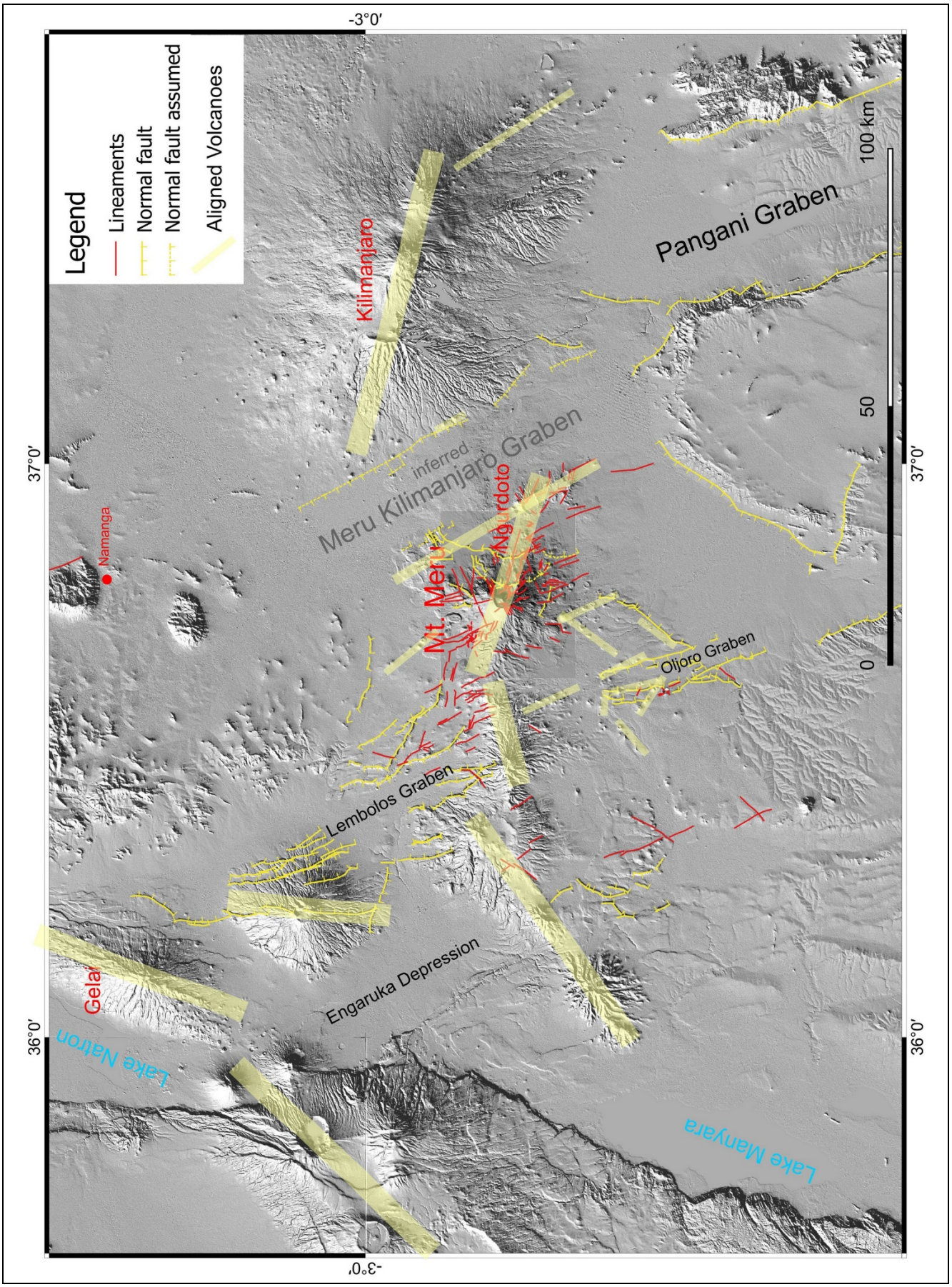

Figure 5.16: Overview of Graben structures (most are NW-oriented), faults and fault-related volcanic-chains of the expanded working area over shaded relief DEMs.

5.3 Lake Momella

Lake Momella is situated in a direct line of a volcanic-chain. Its round shape fits perfectly to the shapes of the other aligned craters. Lake Momella was directly hit at least twice by tremendous debris avalanches. For these reasons, it can strongly be assumed, that it represents a former cone/crater, which was overridden and eroded by the debris avalanches.

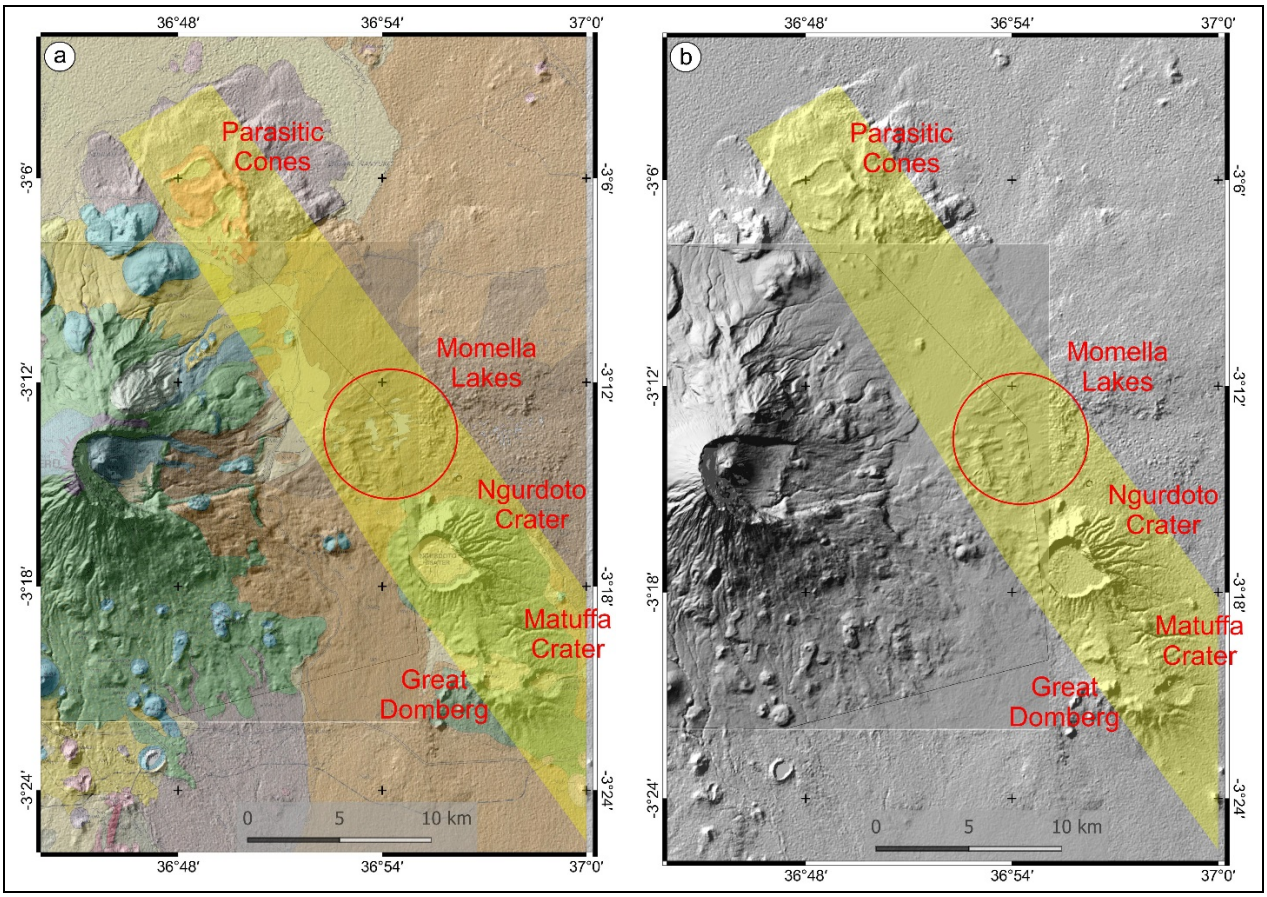

Figure 5.17: Lake Momella is situated in a direct line of a volcanic-chain. It represents very likely a former cone/crater, which was overridden and eroded by the debris avalanches. a: Geological map (WILKINSON, P. ET AL., 1983) over shaded relief DEMs. b: Shaded relief DEMs.

6 Conclusions

East of Mt. Meru an intersection of many different fault orientations can be found. Hence, this location can be considered as highly permeable for groundwater (besides locations with occurrences of porous volcanites) and other fluids and is possibly a location for further examinations. Also at this location, one maximum of subsidence as detected by InSAR studies, occurs (out of several more existing; see report “Ground movements at Mt. Meru detected by InSAR”, in process).

Fault orientations east of Mt. Meru:

- WNW orientation is dominant and connected with young hydrothermal alterations in the central ash cone,
- NW (Pangani Rift, Oljoro Graben, Lembolos Graben, Engaruka Depression, inferred “Mt. Meru Kilimanjaro Graben“,
- NE (Eyasi Rift),
- NNE (Natron-Manyara Rift).

Further findings:

- Two major normal faults at the eastern flank of Mt. Meru possibly triggered the 1) Ngare Nanyuki/Ongadongishu Lahar (reinterpreted as debris avalanche) and led to the collapse of the eastern flank and 2) the Momella Lahar (reinterpreted as debris avalanche).
- A “Mt. Meru Kilimanjaro Graben” can be inferred between these two mountains. It possibly represents the prolongation of the “Kilimanjaro-deflected” Pangani Rift.
- Lake Momella represents very likely a former, now (debris avalanche-) eroded crater.

7 References

BEECKMANS, B. (2014): Volcanism in Tanzania. Thesis, Atlantic International University Honolulu, Hawaii.

DAWSON, J.B. (2008): The Gregory rift valley and Neogene-Recent volcanoes of northern Tanzania: Geological Society of London Memoir 33, 112 p.

DELCAMP, A., DELVAUX, D., KWELWA, S., MACHEYEKI, A. AND KERVYN, M. (2016): Sector collapse events at volcanoes in the North Tanzanian divergence zone and their implications for regional tectonics. Geological Society of America Bulletin, published online on 30 June 2015 as doi:10.1130/B31119.1.

FOSTER ET, A., EBINGER, C., MBEDE, E., & REX, D. (1997): Tectonic development of the northern Tanzanian sector of the East African Rift System. Journal of the Geological Society, London, Vol. 154, pp. 689–700.

LE GALL, B., NONNOTTE, P., ROLET, J., BENOIT, M., GUILLOU, H., MOUSSEAU-NONNOTTE, M., ALBARIC, J., AND DÉVERCHÈRE, J., (2008): Rift propagation at craton margin: Distribution of faulting and volcanism in the North Tanzanian divergence (East Africa) during Neogene times. Tectonophysics, v. 448, no. 1–4, p. 1–19, doi: 10 .1016/j .tecto .2007 .11 .005.

MUIRHEAD, J. D., KATTENHORN, S. A. AND LE CORVEC, N. (2015): Varying styles of magmatic strain accommodation across the East African Rift. Geochemistry, Geophysics, Geosystems, AGU Publications. 2775-2795.

QUENNELL, A. M., MCKINLEY, A.C., AND AITKEN, W.G. (1956): Summary of the Geology of Tanganyika, Part 1. Introduction and stratigraphy, Government Printer, Dar es salaam.

ROBERTS, M. A. (2002): The Geochemical and Volcanological Evolution of the Mt. Meru Region, Northern Tanzania. Dissertation, University of Cambridge, United Kingdom, Christ´s College 2002.

SIEBERT, L., (1984): Large volcanic debris avalanches: Characteristics of source areas, deposits, and associated eruptions: Journal of Volcanology and Geothermal Research, v. 22, p. 163–197, doi: 10 .1016 /0377 -0273 (84)90002 -7.

WILKINSON, P. ET AL. (1983): Geological Map, Arusha Quarter Degree Sheet 55; Geological Survey of Tanzania.

Appendix

Waypoints of measurements and field photos as mentioned in figures. The datum of the coordinates (digital degree) is WGS84.

WP No.	X (longitude)	Y (latitude)	Altitude (m asl)	Date
1	36.8469790	-3.2378810	1623.3	18.10.2016 15:19
2	36.8286500	-3.2444810	1928.3	19.10.2016 14:58
3	36.7870400	-3.2463260	2615.1	19.10.2016 17:02
4	36.7857520	-3.2473400	2612.2	19.10.2016 17:24
5	36.7995360	-3.2292860	2495.4	20.10.2016 07:02
6	36.7864670	-3.2351490	2620.9	20.10.2016 09:13
7	36.7871110	-3.2306770	2638.9	20.10.2016 09:47
8	36.7780820	-3.2316020	2848.3	20.10.2016 11:01
9	36.7660990	-3.2291450	3355.6	20.10.2016 13:17
10	36.7634190	-3.2367580	3589.4	20.10.2016 14:37
11	36.7625870	-3.2369910	3594.9	20.10.2016 14:46
12	36.7620960	-3.2367770	3597.4	20.10.2016 15:04
13	36.7862270	-3.2427500	2571.2	21.10.2016 09:55
14	36.7856790	-3.2437010	2582.9	21.10.2016 10:02
15	36.7852510	-3.2492120	2615.1	21.10.2016 10:27
16	36.7849570	-3.2486600	2595.9	21.10.2016 10:41
17	36.7827680	-3.2509200	2578.4	21.10.2016 11:10
18	36.7894790	-3.2451900	2557.7	21.10.2016 13:18
19	36.6399640	-3.4425150	1222.2	22.10.2016 11:40
20	36.6088480	-3.5114040	1262.8	22.10.2016 12:22
21	36.6068540	-3.5204910	1235.9	22.10.2016 13:09
22	36.6069590	-3.5204840	1240.2	22.10.2016 13:23
23	36.6081160	-3.5227050	1253.9	22.10.2016 13:35
24	36.6036030	-3.5296210	1246.9	22.10.2016 14:00
25	36.6019630	-3.5287530	1209.7	22.10.2016 14:21
26	36.6012590	-3.5282940	1187.8	22.10.2016 14:32
GateMomella	36.8498200	-3.2336210	1601.4	19.10.2016 14:29
Hotspring	37.1937730	-3.4439540	853.5	23.10.2016 11:14
Hut	36.7996460	-3.2294430	2506.5	19.10.2016 18:41
Joined River	36.8056580	-3.2482190	2229.4	21.10.2016 14:47
Lake Momella	36.8915350	-3.2220840	1452.2	18.10.2016 17:08
Lake Momella, Big	36.9058870	-3.2195040	1451.0	18.10.2016 17:24
Mungu Crater	36.6058460	-3.5252720		
Swamp	36.8332670	-3.2468910	1892.9	19.10.2016 14:48
Tanapa	36.6547320	-3.3756560	1375.0	18.10.2016 11:54
View Ngurdoto	36.7917120	-3.2422540	2488.0	19.10.2016 16:14

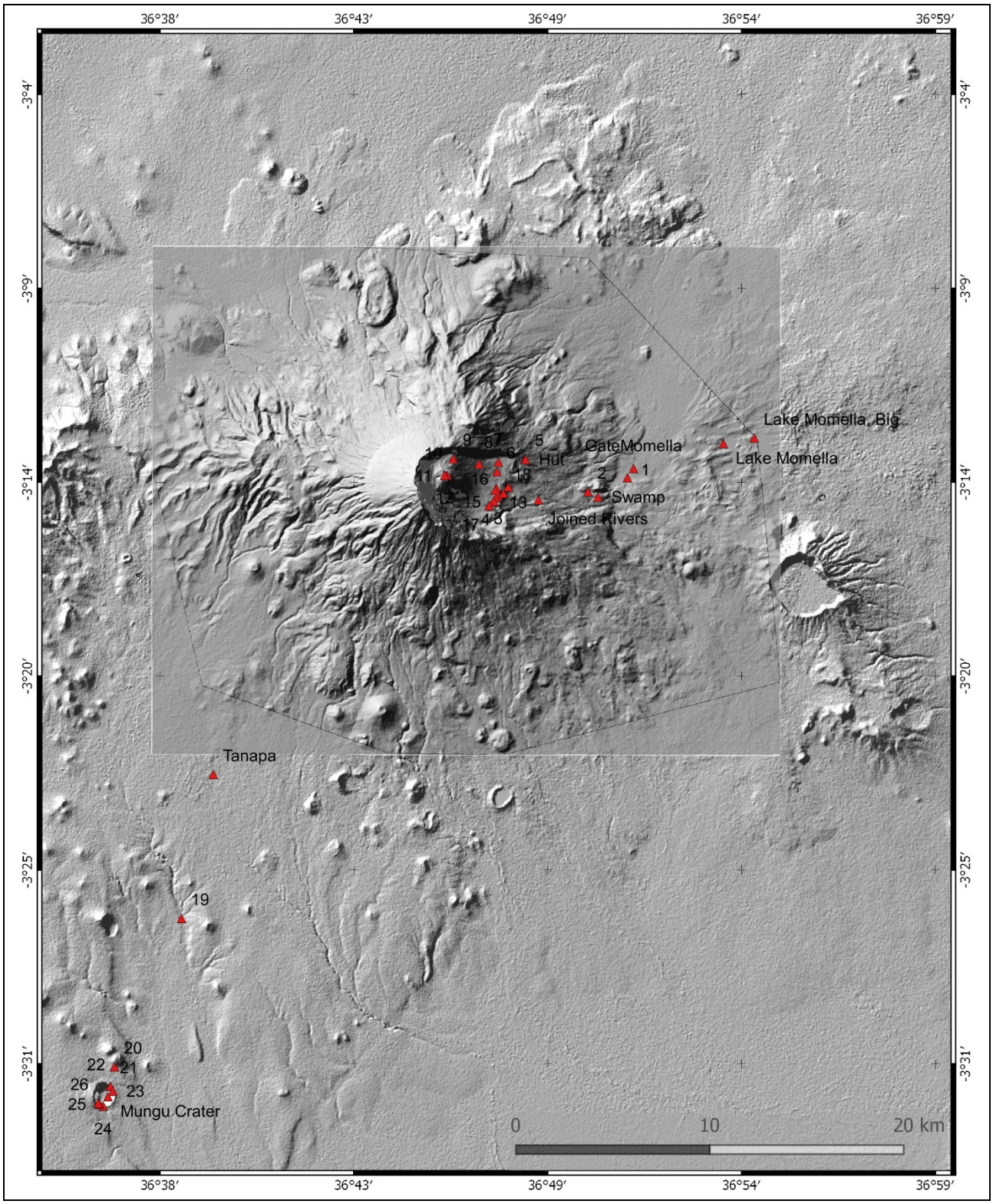

Waypoints of the working area projected into SRTM and TSX WorldDEM elevation model.